

## Casimir Energy of 5D Electromagnetism and New Regularization Based on Minimal-Area Principle

Shoichi ICHINOSE<sup>\*)</sup>

*Laboratory of Physics, School of Food and Nutritional Sciences, University of  
Shizuoka,  
Shizuoka 422-8526, Japan*

(Received November 8, 2008; revised ????? ?, 2009)

We examine the Casimir energy of 5D electromagnetism from the recent standpoint. The bulk geometry is flat. The  $Z_2$  symmetry and periodic property, for the extra coordinate, are taken into account. After confirming the consistency with the past result, we do new things based on a *new regularization*. In the treatment of the divergences, we introduce IR and UV cutoffs and *restrict* the (4D momentum, extra coordinate)-integral region. The regularized configuration is the *sphere lattice*, in the 4D continuum space, which changes along the extra coordinate. The change (renormalization flow) is specified by the *minimal area principle*; hence, this regularization configuration is stringlike. We do the analysis not in the Kaluza-Klein expanded form but in a *closed* form. We do *not* use any perturbation. The formalism is based on the heat-kernel approach using the *position/momentum propagator*. Interesting relations between the heat kernels and the P/M propagators are obtained, where we introduce the *generalized* P/M propagators. A useful expression of the Casimir energy, in terms of the P/M propagator, is obtained. The restricted region approach is replaced by the weight-function approach in the latter-half description. Its meaning, in relation to *space-time quantization*, is argued. *Finite* Casimir energy is numerically obtained. The compactification-size parameter (periodicity) suffers from the renormalization effect. Numerical evaluation is exploited. In particular, the minimal surface lines in the 5D flat space are obtained both numerically using the Runge-Kutta method and analytically using a general solution.

### §1. Introduction

As a unified theory of the four forces in nature, higher-dimensional models have a long history since the papers by Kaluza<sup>1)</sup> and Klein.<sup>2)</sup> The simplest one unifies the forces of gravitons, photons and dilatons. The quantum effects are evaluated by Appelquist and Chodos.<sup>3)</sup> They evaluated Casimir energy<sup>\*\*)</sup> and the result has been giving us a standard image of the contraction of the extra space, that is, when compactification takes place, the extra space shrinks to a size slightly larger than the Planck length.

Higher-dimensional models have, at present, the defect that they, by themselves, are *unrenormalizable*. In Ref.3), UV divergence appears as quintic divergence  $\Lambda^5$  of the *cosmological term*. It simply means that we have no appropriate procedure for defining physical quantities within the quantum field theory (QFT). One can, at this point, have the standpoint that they are effective theories that should be derived from more fundamental models such as the string theory, M-theory, and D-brane. In

---

<sup>\*)</sup> E-mail: ichinose@u-shizuoka-ken.ac.jp

<sup>\*\*)</sup> For a recent review, see Ref.4).

the present study, we pursue the possibility that there is an appropriate procedure for defining physical quantities within the higher-dimensional QFT. We propose a procedure and show that it works well.

There are some approaches to solving the above problem. One of them is the deconstruction model.<sup>5),6)</sup> We discretize the extra coordinate and choose an appropriate finite number of “branes” keeping gauge invariance. This is a commonly used approach at present. Some interesting results are reported.<sup>7),8)</sup> The other approach is based on the regularization using a position-dependent cutoff.<sup>9)</sup> The integral region is restricted appropriately. The restriction requirement comes from the analysis of propagator behaviour.<sup>9),10)</sup> Spiritually, the *holograpy* idea is behind the restriction procedure. The present motivation comes from the question, “Can we find the reason why the restriction process is necessary within the framework of the 5D QFT, not using the string theory and related supergravity theories?”

We introduce a *new* regularization inspired by the partial success of Randall-Schwartz’s result. We associate the regularization (in 4D world) cutoffs running along the extra axis  $y$ , with the *minimal area surfaces* in the bulk. In this way, the stringlike (surface) configuration (closed string) is introduced in the present approach. This is quite in contrast to the usual string theory approach. The present stringlike configuration appears not from the propagation of strings but from the necessity of the restriction of the integral region in the bulk space.

The original approach to the renormalization flow interpretation of bulk behaviour relies on the AdS/CFT and 5D supergravity.<sup>11)–16)</sup> The present approach does *not* rely on them. We *directly* use the minimal area principle, the essence of the string theory,<sup>17)–19)</sup> in the *regularization procedure*. This is *new* in the development of the quantum field theory.

This paper is organized as follows. In §2, we review the 5D quantum electromagnetism in the recent standpoint. Casimir energy is obtained from the KK-expansion approach. In §3, the same quantity of §2 is dealt with in the heat-kernel method, and Casimir energy is expressed in a closed form in terms of the P/M propagator. The closed expression of Casimir energy is numerically evaluated and its equivalence with the result of §2 is confirmed in §4. Here we introduce UV and IR regularization parameters in the(4D momentum, extra coordinate) space. A new idea about UV and IR regularization is presented in §5. The minimal surface principle is introduced. The *sphere lattice* and *renormalization* are explained. In §6, an improved regularization procedure is presented where a *weight function* is introduced. Here, again the *minimal surface principle* is taken. The definition of the weight function is given in §7. In §8, we present the conclusions. We prepare two appendices to supplement the text. Appendix A deals with the analytic solution of the minimal surface curve in the 5D flat space. Appendix B provides an explanation of the numerical confirmation of the (approximate) equality of the minimal surface curve and the dominant path in Casimir energy calculation.

## §2. Five-dimensional quantum electromagnetism

We consider the flat 5D space-time  $(X^M) = (x^\mu, y)$  with the periodicity in the extra space  $y$ ,

$$\begin{aligned} ds^2 &= \eta_{\mu\nu} dx^\mu dx^\nu + dy^2 \quad , \quad -\infty < y < \infty \quad , \quad y \rightarrow y + 2l, \\ (\eta_{\mu\nu}) &= \text{diag}(-1, 1, 1, 1) \quad , \quad (X^M) = (x^\mu, x^5 = y) \equiv (x, y) \quad , \\ &M, N = 0, 1, 2, 3, 5; \quad \mu, \nu = 0, 1, 2, 3. \end{aligned} \quad (2.1)$$

The 5D electromagnetism is described by the 5D U(1) gauge field  $A_M$ ,

$$\begin{aligned} S_{EM} &= \int d^4x dy \sqrt{-G} \left\{ -\frac{1}{4} F_{MN} F^{MN} \right\} \equiv \int d^4x dy \mathcal{L}_{EM} \quad , \quad G = \det G_{MN} \quad , \\ &F_{MN} = \partial_M A_N - \partial_N A_M \quad , \quad (X^M) = (x^\mu, y) \quad , \\ ds^2 &= G_{MN} dX^M dX^N \quad , \quad (G_{MN}) = \text{diag}(-1, 1, 1, 1, 1) \end{aligned} \quad (2.2)$$

It has U(1) gauge symmetry,

$$A_M \rightarrow A_M + \partial_M \Lambda \quad , \quad (2.3)$$

where  $\Lambda(X)$  is the 5D gauge parameter.

We respect  $Z_2$  symmetry in the extra space,

$$y \rightarrow -y \quad . \quad (2.4)$$

The  $Z_2$  parity assignment of  $A_M(x^\mu, y)$  is fixed by the 5D gauge transformation (2.3). There are two cases corresponding to the choice of the  $Z_2$  parity of  $\Lambda(x^\mu, y)$ ,

$$\begin{aligned} \text{Case 1. Even-parity case} \quad & \Lambda(x^\mu, y) = +\Lambda(x^\mu, -y) \\ & A_\mu : P = + \quad , \quad A_5 : P = - \quad , \\ \text{Case 2. Odd-parity case} \quad & \Lambda(x^\mu, y) = -\Lambda(x^\mu, -y) \\ & A_\mu : P = - \quad , \quad A_5 : P = + \quad . \end{aligned} \quad (2.5)$$

In the present paper, we consider Case 1. (Case 2 can be similarly treated.)

We take the following gauge-fixing term to quantize the present system. \*)

$$\begin{aligned} \mathcal{L}_g &= -\frac{1}{2} (\partial_M A^M)^2 = -\frac{1}{2} (\partial_\mu A^\mu + \partial_y A^5)^2 \quad , \\ \mathcal{L}_{EM} + \mathcal{L}_g &= \frac{1}{2} A_\mu (\partial^2 + \partial_y^2) A^\mu + \frac{1}{2} A^5 (\partial^2 + \partial_y^2) A^5 + \text{total derivatives} \quad , \end{aligned} \quad (2.6)$$

where  $\partial^2 \equiv \partial_\mu \partial^\mu$ . Then the field equations are given by

$$(\partial^2 + \partial_y^2) A^\mu = 0 \quad , \quad (\partial^2 + \partial_y^2) A^5 = 0 \quad . \quad (2.7)$$

---

\*) The gauge independence of the physical quantities is an important check point of the proposal in the present paper. We relegate it to a future work. The gauge independence of Casimir energy of the 5D KK theory (Appelquist and Chodos's result<sup>3)</sup>) was confirmed in Ref.<sup>20)</sup>

We consider the system in the periodic condition(2.1). Then we can write  $A^M$  as

$$\begin{aligned} A^\mu(x, y) &= a_0^\mu(x) + 2 \sum_{n=1}^{\infty} a_n^\mu(x) \cos \frac{n\pi}{l} y \quad , \quad P=+ \\ A^5(x, y) &= 2 \sum_{n=1}^{\infty} b_n(x) \sin \frac{n\pi}{l} y \quad , \quad P=- \quad , \end{aligned} \quad (2.8)$$

where  $\{a_n^\mu(x)\}$  and  $\{b_n(x)\}$  are the KK-expansion coefficients. From Eq.(2.7), they satisfy

$$\partial^2 a_0^\mu = 0 \quad (\text{zero mode}), \quad \{\partial^2 - (\frac{n\pi}{l})^2\} a_n^\mu = 0, \quad \{\partial^2 - (\frac{n\pi}{l})^2\} b_n = 0, \quad n \neq 0. \quad (2.9)$$

The on-shell condition, Eq.(2.7) or Eq.(2.9), is for the analysis of the S-matrix. In this study, we do not use the condition. \*) The total action can be written as

$$\begin{aligned} & \int_{-l}^l dy (\mathcal{L}_{EM} + \mathcal{L}_g) = \\ & 2l \left\{ \frac{1}{2} \sum_{n \in \mathbf{Z}} a_{n\mu} \left( \partial^2 - \left( \frac{n\pi}{l} \right)^2 \right) a_n^\mu + \frac{1}{2} \sum_{n \in \mathbf{Z}, n \neq 0} b_n \left( \partial^2 - \left( \frac{n\pi}{l} \right)^2 \right) b_n \right\}. \end{aligned} \quad (2.11)$$

Then Casimir energy  $E_{Cas}$  is given by \*\*)

$$\begin{aligned} e^{-l^4 E_{Cas}} &= \int \prod_{n, \mu} \mathcal{D}a_n^\mu \prod_{m \neq 0} db_m \exp i \int d^4 x dy (\mathcal{L}_{EM} + \mathcal{L}_g) \\ &= \exp \left[ -\frac{1}{2} l^4 \int \frac{d^4 p}{(2\pi)^4} \left\{ 4 \sum_{n \in \mathbf{Z}} \ln(p^2 + m_n^2) + \sum_{n \in \mathbf{Z}, n \neq 0} \ln(p^2 + m_n^2) \right\} \right] \end{aligned} \quad (2.12)$$

---

\*) We do not take into account the degree of freedom  $5-2=3$  among five components  $\{A^M\}$  due to the local gauge symmetry. This is because we will compare the present results of the flat geometry with those of the warped geometry. In the latter treatment, we start with the *massive* vector theory that has no local gauge symmetry.<sup>9)</sup>

$$S_{5dV} = \int d^4 x dz \sqrt{-G} \left( -\frac{1}{4} F_{MN} F^{MN} - \frac{1}{2} m^2 A^M A_M \right), \quad (2.10)$$

The 5D mass parameter  $m$  is regarded as an IR-regularization parameter. The 5D gauge theory is the limit  $m = 0$ . For the general  $m$ , Casimir energy is some integral of the (modified) Bessel functions with the number  $\nu = \sqrt{1 + m^2/\omega^2}$  where  $\omega$  is the warp parameter. The simplest case for analysis is not  $m = 0$  but  $m = i\omega$ . UV behaviour, which is the key point of the present paper, is considered independent of the IR regularization parameter  $m$ . Hence, the massive case is (practically) important for the 5D theories. We also include the longitudinal component to respect the manifest 5D Lorentz invariance. For the later use of the comparison with the warped case, we consider, instead of the 5D EM, the system of four 5D massless scalars with the even parity and one with the odd parity.

\*\*) Casimir energy is defined to be the free part (independent of the coupling) of vacuum energy that depends on the *boundary*. The quantity is defined to be the energy per unit space-volume of the ‘‘brane’’. In the present model of 3-brane (3+1 dim real world), space-volume has the dimension of  $L^3$ . Hence the dimension of  $E_{Cas}$  is  $L^{-4}$ .

where  $p^2 \equiv p_\mu p^\mu$  and  $m_n = \frac{n\pi}{l}$ . This expression is the standard one. The above KK-summation and  $p_\mu$  integral are divergent, hence we must regularize them. The standard way taken by Appelquist and Chodos<sup>3)</sup> goes as follows. It is sufficient to consider the even-parity quantity.

$$V(l) = \frac{1}{2} \int \frac{d^4 p}{(2\pi)^4} \sum_{n \in \mathbf{Z}} \ln(p^2 + m_n^2) \quad . \quad (2.13)$$

This is the (unregularized) Casimir energy for one scalar mode with  $Z_2$ -parity even. The first step is to introduce a reference point  $l_0$ .

$$V(l) - V(l_0) = \frac{1}{2} \int \frac{d^4 p}{(2\pi)^4} \sum_{n \in \mathbf{Z}} \ln \frac{(p^2 + (\frac{n\pi}{l})^2)}{(p^2 + (\frac{n\pi}{l_0})^2)} \quad . \quad (2.14)$$

This procedure makes us drop the  $l$ -independent quantity. Using the well-known formula

$$\sum_{n=-\infty}^{\infty} f_n = \int_{-\infty}^{\infty} dz f(z) + \int_{-\infty+i\epsilon}^{+\infty+i\epsilon} dz \frac{f(z) + f(-z)}{e^{-2\pi iz} - 1} \quad , \quad (2.15)$$

the KK-sum in Eq.(2.14) is replaced by the  $z$ -integral:

$$\frac{1}{2} \int \frac{d^4 p}{(2\pi)^4} \left[ \int_{-\infty}^{\infty} dz \ln \frac{p^2 + (\frac{z\pi}{l})^2}{p^2 + (\frac{z\pi}{l_0})^2} + \int_{-\infty+i\epsilon}^{+\infty+i\epsilon} dz \frac{2 \ln \frac{p^2 + (\frac{z\pi}{l})^2}{p^2 + (\frac{z\pi}{l_0})^2}}{e^{-2\pi iz} - 1} \right] \quad . \quad (2.16)$$

We consider the spacelike 4D momentum  $p_\mu$ :  $p^2 = p_\mu p^\mu > 0$ . Using the second formula,

$$\int_{-\infty}^{\infty} dz H(z) \ln \frac{z^2 + a^2}{z^2 + b^2} = 2\pi \int_b^a dx H(ix) \quad , \quad (2.17)$$

the first part of (2.16) is evaluated as

$$\frac{1}{2} \int \frac{d^4 p}{(2\pi)^4} \int_{-\infty}^{\infty} dz \ln \frac{(p^2 + (\frac{z\pi}{l})^2)}{(p^2 + (\frac{z\pi}{l_0})^2)} = (l - l_0) \int \frac{d^4 p}{(2\pi)^4} \sqrt{p^2} \quad . \quad (2.18)$$

This integral is quintically divergent, but turns out to be cancelled out, as shown below. As for the second part, the integrand of the  $p$ -integral, using Eq.(2.17) again, is evaluated as

$$\begin{aligned} \int_{-\infty}^{\infty} dz \frac{\ln \frac{(p^2 + (\frac{z\pi}{l})^2)}{(p^2 + (\frac{z\pi}{l_0})^2)}}{e^{-2\pi iz} - 1} &= 2\pi \int_{\frac{l_0}{\pi}\sqrt{p^2}}^{\frac{l}{\pi}\sqrt{p^2}} \frac{1}{e^{2\pi x} - 1} dx \\ &= -\sqrt{p^2}(l - l_0) + \ln \frac{e^{l\sqrt{p^2}} - e^{-l\sqrt{p^2}}}{e^{l_0\sqrt{p^2}} - e^{-l_0\sqrt{p^2}}} \quad . \end{aligned} \quad (2.19)$$

We see that the first term in the above final expression, after the  $p$ -integral, cancel the quintically divergent one (2.18). Hence, we finally obtain

$$\begin{aligned} V(l) - V(l_0) &= \int \frac{d^4 p}{(2\pi)^4} \ln \frac{e^{l\sqrt{p^2}} - e^{-l\sqrt{p^2}}}{e^{l_0\sqrt{p^2}} - e^{-l_0\sqrt{p^2}}} \\ &= \frac{1}{8\pi^2} \frac{1}{l^4} \int_0^\infty dk k^3 \left\{ k + \ln(1 - e^{-2k}) - \frac{l_0}{l} k - \ln(1 - e^{-\frac{2l_0}{l}k}) \right\}, (l\sqrt{p^2} \equiv k). \end{aligned} \quad (2.20)$$

Using the third formula

$$\int_0^\infty dk k^3 \ln(1 - e^{-2k}) = -\frac{3}{4}\zeta(5) \quad , \quad (2.21)$$

we obtain

$$\begin{aligned} 8\pi^2[V(l) - V(l_0)] &= \\ \left(1 - \frac{l_0}{l}\right) \frac{1}{l^4} \int_0^\infty dk k^4 + \frac{1}{l^4} \left\{ -\frac{3}{4}\zeta(5) + \left(\frac{l}{l_0}\right)^4 \cdot \frac{3}{4} \cdot \zeta(5) \right\} \quad . \end{aligned} \quad (2.22)$$

The first term is *quintically* divergent. We take, as the (dimensionless) UV *cutoff* of the  $k$ -integral,  $l\Lambda$  then

$$8\pi^2[V(l) - V(l_0)] = \frac{1}{5}l\Lambda^5 - \frac{3}{4}\frac{\zeta(5)}{l^4} - \left(\frac{1}{5}l_0\Lambda^5 - \frac{3}{4}\frac{\zeta(5)}{(l_0)^4}\right) \quad . \quad (2.23)$$

Hence, we obtain Casimir energy and Casimir force for the simple system Eq.(2.13) as

$$\begin{aligned} 8\pi^2 \times V(l) &= \frac{1}{5}l\Lambda^5 - \frac{3}{4}\frac{\zeta(5)}{l^4}, \quad F_{Cas}^A(l) = -\frac{\partial V}{\partial l} = \left(-\frac{1}{5}\Lambda^5 - 3\frac{\zeta(5)}{l^5}\right) \frac{1}{8\pi^2}, \\ &\zeta(5) = 1.03693 \dots \quad . \end{aligned} \quad (2.24)$$

The first term of  $V(l)$  is *quintically* divergent but is simply proportional to  $l$ . This quantity comes from the *UV divergences* of 5D quantum fluctuation. In Casimir force  $F_{Cas}^A = -\frac{\partial V}{\partial l}$ , that part does not depend on  $l$ . If we can find a right means of avoiding the UV divergences (which will be proposed later) we may drop the (divergent) constant contribution, and we obtain Casimir force for the 5D electromagnetism as

$$F_{Cas} = 5 \times \left(-3\frac{\zeta(5)}{l^5}\right) \times \frac{1}{8\pi^2} \quad . \quad (2.25)$$

The minus sign denotes the *attractive* force.

### §3. Heat-kernel approach and position/momentum propagator

We reformulate the previous section using a heat kernel in order to treat the problem *without* KK expansion. Note that the heat-kernel method is a complete quantization procedure for the free theory (quadratic theory).<sup>21)</sup> Instead of the

5D gauge fields  $A^M(X)$ , we introduce partially Fourier-transformed ones  $A_p^M(y) = (A_p^\mu(y), B_p(y))$ .

$$\begin{aligned} A^\mu(x, y) &= \int \frac{d^4 p}{(2\pi)^4} e^{ipx} A_p^\mu(y) \quad : \quad P=+ \quad , \\ A^5(x, y) &= \int \frac{d^4 p}{(2\pi)^4} e^{ipx} B_p(y) \quad : \quad P=- \quad . \end{aligned} \quad (3.1)$$

(We do *not* Fourier-transform the extra space ( $y$ ) part.) Then the total action is given by

$$\begin{aligned} S &= \int d^4 x dy (\mathcal{L}_{EM} + \mathcal{L}_g) \\ &= \int \frac{d^4 p}{(2\pi)^4} \int_{-l}^l dy \left[ \frac{1}{2} A_{\mu p}(y) (-p^2 + \partial_y^2) A_p^\mu(y) + \frac{1}{2} B_p(y) (-p^2 + \partial_y^2) B_p(y) \right]. \end{aligned} \quad (3.2)$$

Here we restrict the  $y$ -integral region to  $[-l, l]$  because it has sufficient information and can be transformed (by the Fourier expansion) to the periodic form defined in  $(-\infty, +\infty)$ . The on-shell condition is given by

$$\begin{aligned} (-p^2 + \partial_y^2) A_p^\mu(y) &= 0 \quad , \quad -l \leq y \leq l \quad , \quad P=+ \\ (-p^2 + \partial_y^2) B_p(y) &= 0 \quad , \quad -l \leq y \leq l \quad , \quad P=- \quad . \end{aligned} \quad (3.3)$$

This condition, which is *not* used in the following, is necessary when we consider the S-matrix. Casimir energy  $E_{Cas}$  is given by

$$\begin{aligned} e^{-l^4 E_{Cas}} &= \int \mathcal{D}A_{\mu p} \mathcal{D}B_p \exp\{iS\} \\ &= \exp l^4 \int \frac{d^4 p}{(2\pi)^4} \frac{1}{2l} \int_{-l}^l dy \left\{ -\frac{4}{2} \ln(p^2 - \partial_y^2) - \frac{1}{2} \ln(p^2 - \partial_y^2) \right\} \quad . \end{aligned} \quad (3.4)$$

Using the following formula<sup>21)</sup>

$$\int_0^\infty \frac{e^{-t} - e^{-tM}}{t} dt = \ln M \quad , \quad \det M > 0 \quad , \quad M : \text{a matrix} \quad , \quad (3.5)$$

we can *formally* write

$$-\ln(p^2 - \partial_y^2) = \int_0^\infty \frac{1}{t} e^{-t(p^2 - \partial_y^2)} dt + \text{divergent constant} \quad , \quad (3.6)$$

where the divergent constant should not depend on  $p$  or  $y$ . We understand that  $M$  in Eq.(3.5) is the matrix  $M_{y, y'}$  labeled by the continuous parameters  $y$  and  $y'$  and that  $(p^2 - \partial_y^2)$  in Eq.(3.6) is the differential operator acting on  $|y \rangle$ , a quantum state labeled by the position  $y$ . <sup>\*</sup>) The heat kernels  $H_p$  and  $E_p$  are in an abstract

---

<sup>\*</sup>)  $\langle y|$  and  $|y \rangle$  are introduced by Dirac<sup>22)</sup> and are called the bra and ket vectors respectively. It is defined by the orthonormal eigenfunctions of the kinetic differential operator of the system. When we take the orthogonality relation  $\langle y|y' \rangle = \hat{\delta}(y - y')$ , their physical dimensions are  $[-y_i] = L^{-\frac{1}{2}}$  and  $[|y \rangle] = L^{-\frac{1}{2}}$ .

way defined by

$$\begin{aligned} \overline{H}_p(y, y'; t) &= \langle y | e^{-(p^2 - \partial_y^2)t} | y' \rangle \Big|_{P=-} , \\ E_p(y, y'; t) &= \langle y | e^{-(p^2 - \partial_y^2)t} | y' \rangle \Big|_{P=+} . \end{aligned} \quad (3.7)$$

Hence, we obtain the final expression of  $E_{Cas}$ :

$$e^{-l^4 E_{Cas}} = (\text{const}) \times \exp \left[ l^4 \int \frac{d^4 p}{(2\pi)^4} \int_0^\infty \frac{dt}{t} \left\{ \frac{4}{2} \text{Tr} E_p(y, y'; t) + \frac{1}{2} \text{Tr} H_p(y, y'; t) \right\} \right] , \quad (3.8)$$

where Tr represents the integral over all  $y = y'$  values. \*)

$$\text{Tr} E_p(y, y'; t) = \int_{-l}^l dy E_p(y, y; t), \quad \text{Tr} H_p(y, y'; t) = \int_{-l}^l dy H_p(y, y; t). \quad (3.11)$$

The precise definitions of  $H_p$  and  $E_p$ , with the initial condition (3.14) shown below, are given by the *heat equations*,

$$\begin{aligned} \left\{ \frac{\partial}{\partial t} + p^2 - \partial_y^2 \right\} H_p(y, y'; t) &= 0 \quad , \quad P = - \quad , \\ \left\{ \frac{\partial}{\partial t} + p^2 - \partial_y^2 \right\} E_p(y, y'; t) &= 0 \quad , \quad P = + \quad . \end{aligned} \quad (3.12)$$

The solutions are, in terms of the KK-eigen-functions, given by

$$\begin{aligned} H_p(y, y'; t) &= \frac{1}{2l} \sum_{n \in \mathbf{Z}} e^{-(k_n^2 + p^2)t} \frac{1}{2} \{ e^{-ik_n(y-y')} - e^{-ik_n(y+y')} \} \quad , \\ E_p(y, y'; t) &= \frac{1}{2l} \sum_{n \in \mathbf{Z}} e^{-(k_n^2 + p^2)t} \frac{1}{2} \{ e^{-ik_n(y-y')} + e^{-ik_n(y+y')} \} \quad , \\ k_n &= \frac{n\pi}{l} \quad , \end{aligned} \quad (3.13)$$

where we use the dimensionalities of  $H_p$  and  $E_p$  read from (3.8);  $[E_p] = [H_p] = L^{-1}$ .

---

\*) For the 5D free scalar with  $Z_2$ -parity even, Casimir energy is given by

$$e^{-l^4 E_{Cas}} = (\text{const}) \times \exp \left[ l^4 \int \frac{d^4 p}{(2\pi)^4} \int_0^\infty \frac{dt}{t} \frac{1}{2} \text{Tr} E_p(y, y'; t) \right] \quad , \quad (3.9)$$

and, for that with  $Z_2$ -parity odd,

$$e^{-l^4 E_{Cas}} = (\text{const}) \times \exp \left[ l^4 \int \frac{d^4 p}{(2\pi)^4} \int_0^\infty \frac{dt}{t} \frac{1}{2} \text{Tr} H_p(y, y'; t) \right] \quad , \quad (3.10)$$



\*\*\*) The above heat kernels satisfy the following b.c.,

$$\begin{aligned}\lim_{t \rightarrow +0} H_p(y, y'; t) &= \frac{1}{2l} \sum_{n \in \mathbf{Z}} \frac{1}{2} \{e^{-ik_n(y-y')} - e^{-ik_n(y+y')}\} \\ &= \frac{1}{2} \{\hat{\delta}(y-y') - \hat{\delta}(y+y')\} \quad , \\ \lim_{t \rightarrow +0} E_p(y, y'; t) &= \frac{1}{2l} \sum_{n \in \mathbf{Z}} \frac{1}{2} \{e^{-ik_n(y-y')} + e^{-ik_n(y+y')}\} \\ &= \frac{1}{2} \{\hat{\delta}(y-y') + \hat{\delta}(y+y')\} \quad ,\end{aligned}\quad (3.14)$$

where we have introduced  $\hat{\delta}(y) \equiv \frac{1}{2l} \sum_{n \in \mathbf{Z}} e^{-ik_n y}$ . With this b.c., the heat equation (3.12) can *rigorously* define  $H_p$  and  $E_p$ . We here introduce the *position/momentum propagators*  $G_p^\mp$  as follows:

$$\begin{aligned}G_p^-(y, y') &\equiv \int_0^\infty dt H_p(y, y'; t) = \frac{1}{2l} \sum_{n \in \mathbf{Z}} \frac{1}{k_n^2 + p^2} \frac{1}{2} \{e^{-ik_n(y-y')} - e^{-ik_n(y+y')}\}, \\ G_p^+(y, y') &\equiv \int_0^\infty dt E_p(y, y'; t) = \frac{1}{2l} \sum_{n \in \mathbf{Z}} \frac{1}{k_n^2 + p^2} \frac{1}{2} \{e^{-ik_n(y-y')} + e^{-ik_n(y+y')}\}.\end{aligned}\quad (3.15)$$

They satisfy the following differential equations of *propagators*:

$$\begin{aligned}(p^2 - \partial_y^2) G_p^\mp(y, y') &= \frac{1}{2l} \sum_{n \in \mathbf{Z}} \frac{1}{2} \{e^{-ik_n(y-y')} \mp e^{-ik_n(y+y')}\} \\ &\equiv \frac{1}{2} \{\hat{\delta}(y-y') \mp \hat{\delta}(y+y')\} \quad ,\end{aligned}\quad (3.16)$$

Therefore, Casimir energy  $E_{Cas}$  is, from Eqs.(3.8) and (3.13), given by

$$\begin{aligned}E_{Cas}(l) &= \int \frac{d^4 p}{(2\pi)^4} \int_0^\infty \frac{dt}{t} 2 \int_0^l dy \left\{ \frac{1}{2} \frac{1}{2l} \sum_{n \in \mathbf{Z}} e^{-(k_n^2 + p^2)t} \frac{1}{2} \{1 - e^{-2ik_n y}\} \right. \\ &\quad \left. + 2 \frac{1}{2l} \sum_{n \in \mathbf{Z}} e^{-(k_n^2 + p^2)t} \frac{1}{2} \{1 + e^{-2ik_n y}\} \right\} \quad .\end{aligned}\quad (3.17)$$

This expression leads to the same treatment as that in the previous section.

Here, we introduce the *generalized* P/M propagators,  $I_\alpha(P=-)$  and  $J_\alpha(P=+)$  as

$$I_\alpha(p^2; y, y') \equiv \int_0^\infty \frac{dt}{t^\alpha} H_p(y, y'; t)$$

---

\*\*) If we ignore the dimensionality,

$$\frac{1}{2l} \sum_{n \in \mathbf{Z}} \{e^{-(k_n^2 + p^2)t} / (k_n^2 + p^2)^s\} \frac{1}{2} \{e^{-ik_n(y-y')} \mp e^{-ik_n(y+y')}\}, \quad s : \text{real number}$$

are the more general solutions of Eq.(3.12).

$$\begin{aligned}
&= \int_0^\infty \frac{dt}{t^\alpha} \frac{1}{2l} \sum_{n \in \mathbf{Z}} e^{-(k_n^2 + p^2)t} \frac{1}{2} \{e^{-ik_n(y-y')} - e^{-ik_n(y+y')}\} \quad , \quad P = - \quad , \\
&\qquad\qquad\qquad J_\alpha(p^2; y, y') \equiv \int_0^\infty \frac{dt}{t^\alpha} E_p(y, y'; t) \\
&= \int_0^\infty \frac{dt}{t^\alpha} \frac{1}{2l} \sum_{n \in \mathbf{Z}} e^{-(k_n^2 + p^2)t} \frac{1}{2} \{e^{-ik_n(y-y')} + e^{-ik_n(y+y')}\} \quad , \quad P = + \quad , \quad (3.18)
\end{aligned}$$

where  $\alpha$  is an arbitrary real number. Then we have the following relations:

$$\begin{aligned}
I_0(p^2; y, y') &= G_p^-(y, y') \quad , \quad J_0(p^2; y, y') = G_p^+(y, y') \quad , \\
\frac{\partial I_\alpha(p^2; y, y')}{\partial p^2} &= -I_{\alpha-1}(p^2; y, y') \quad , \quad \int_{p^2}^\infty dk^2 I_\alpha(k^2; y, y') = I_{\alpha+1}(p^2; y, y') \quad , \\
\frac{\partial J_\alpha(p^2; y, y')}{\partial p^2} &= -J_{\alpha-1}(p^2; y, y') \quad , \quad \int_{p^2}^\infty dk^2 J_\alpha(k^2; y, y') = J_{\alpha+1}(p^2; y, y') \quad , \\
(p^2 - \partial_y^2) I_\beta(p^2; y, y') &= -\beta I_{\beta+1}(p^2; y, y') \quad , \\
(p^2 - \partial_y^2) J_\beta(p^2; y, y') &= -\beta J_{\beta+1}(p^2; y, y') \quad , \beta \neq 0 \quad . \quad (3.19)
\end{aligned}$$

Finally, we obtain the following useful expression of Casimir energy in terms of P/M propagators,

$$\begin{aligned}
E_{Cas}(l) &= \int \frac{d^4 p}{(2\pi)^4} \left\{ \frac{1}{2} \text{Tr} I_1(p^2; y, y') + \frac{4}{2} \text{Tr} J_1(p^2; y, y') \right\} \\
&= \int \frac{d^4 p}{(2\pi)^4} \int_{p^2}^\infty \left\{ \frac{1}{2} \text{Tr} I_0(k^2; y, y') + 2 \text{Tr} J_0(k^2; y, y') \right\} dk^2 \\
&= \int \frac{d^4 p}{(2\pi)^4} \int_{p^2}^\infty \left\{ \frac{1}{2} \text{Tr} G_k^-(y, y') + 2 \text{Tr} G_k^+(y, y') \right\} dk^2 \quad . \quad (3.20)
\end{aligned}$$

Here, we list the dimensions of the various quantities appeared above.

Dim	$L^{1-2\alpha}$	$L^{-4}$	$L^{-3/2}$	$L^{-1}$	$L^{-1/2}$	$L$	$L^2$	$L^{5/2}$
	$I_\alpha, J_\alpha$	$E_{Cas}$	$A^\mu, A^5$	$\mu, \Lambda, p$ $H_p, E_p$	$ \mathbf{y} \rangle, \langle \mathbf{y} $	$\epsilon, l, y$ $G_p^\mp$	$t$	$A_p^\mu, B_p$

( $\Lambda, \mu$ , and  $\epsilon$  are the regularization parameters defined below.)

The P/M propagators  $G_k^\mp$ , which are expressed in Eq.(3.15) in the form of a summation over *all* modes, can be expressed in a *closed* form. (See, for example, Eq.(36) of Ref.10.)

$$\begin{aligned}
G_k^\mp(y, y') &= \pm \frac{\cosh \tilde{k}(|y + y'| - l) \mp \cosh \tilde{k}(|y - y'| - l)}{4\tilde{k} \sinh \tilde{k}l} \quad , \\
-l \leq y \leq l \quad , \quad -l \leq y' \leq l \quad , \quad \tilde{k} &\equiv \sqrt{k_\mu k^\mu} \quad , \quad k_\mu k^\mu > 0(\text{spacelike}) \quad , \quad (3.21)
\end{aligned}$$

where the plural sign means that one corresponds to the other in the same position.

\*) By using the above results, Casimir energy is explicitly written as

$$\begin{aligned}
E_{Cas}(l) &= \int \frac{d^4 p}{(2\pi)^4} \int_0^l dy (F^-(\tilde{p}, y) + 4F^+(\tilde{p}, y)) \quad , \\
F^-(\tilde{p}, y) &\equiv \int_{p^2}^{\infty} dk^2 G_k^-(y, y) = \int_{\tilde{p}}^{\infty} d\tilde{k} \frac{\cosh \tilde{k}(2y-l) - \cosh \tilde{k}l}{2 \sinh(\tilde{k}l)} \quad , \\
F^+(\tilde{p}, y) &\equiv \int_{p^2}^{\infty} dk^2 G_k^+(y, y) = \int_{\tilde{p}}^{\infty} d\tilde{k} \frac{-\cosh \tilde{k}(2y-l) - \cosh \tilde{k}l}{2 \sinh(\tilde{k}l)} \quad . \quad (3.22)
\end{aligned}$$

This is the closed expression, not the expanded one. (In relation to the degree of freedom of the system, the integrands of  $F^\mp$  are, in a later description, graphically shown in Figs.5 and 6.)

#### §4. UV and IR regularization parameters and evaluation of Casimir energy

The integral region of Eq.(3.22) is displayed in Fig. 1. In the figure, we introduce the *UV and IR regularization cutoffs*  $\mu \leq \tilde{p} \leq \Lambda$  and  $\epsilon \leq y \leq l$ . In order to suppress the number of artificial parameters as much as possible, we take the relations \*) :

$$\epsilon = \frac{1}{\Lambda} \quad , \quad \mu = \frac{1}{l} \quad . \quad (4.1)$$

This is the same situation as that in the *lattice gauge theory* ( unit lattice size =  $(1/\Lambda)^4 \times \epsilon = (1/\Lambda)^5$ ; total lattice size =  $(1/\mu)^4 \times l = l^5$ ).

Let us evaluate the  $(\Lambda, l)$ -regularized value of Eq.(3.22).

$$\begin{aligned}
E_{Cas}(\Lambda, l) &= \frac{2\pi^2}{(2\pi)^4} \int_{1/l}^{\Lambda} d\tilde{p} \int_{1/\Lambda}^l dy \tilde{p}^3 F(\tilde{p}, y) \quad , \\
F(\tilde{p}, y) &\equiv F^-(\tilde{p}, y) + 4F^+(\tilde{p}, y) = \int_{\tilde{p}}^{\Lambda} d\tilde{k} \frac{-3 \cosh \tilde{k}(2y-l) - 5 \cosh \tilde{k}l}{2 \sinh(\tilde{k}l)} \quad . \quad (4.2)
\end{aligned}$$

The integral region of  $(\tilde{p}, y)$  is the *rectangle* shown in Fig. 1. We now use the formula of the indefinite integrals:

$$\int \frac{\cosh x}{\sinh x} dx = \ln |\sinh(x)| \quad ,$$

---

\*) The expression of Eq.(3.21) is considered in  $-l \leq y \leq l$ , and the periodicity ( $y \rightarrow y + 2l$ ) seems lost. If, however, we *Fourier-expand* Eq.(3.21) in the interval, the same expression as Eq.(3.15) is obtained. Note that the present treatment is crucially different from the deconstruction approach in that *all* Kaluza-Klein modes are taken into account. The necessity of all the KK modes was stressed in the  $\delta(0)$ -problem of the bulk-boundary theory.<sup>23),24)</sup>

\*) As for the numerical values of  $\Lambda$  and  $l$ , they depend on the chosen energy unit ( e.g. eV and J) and the physical model concerned. For example, if we consider the grand unified theories,  $\Lambda = 10^{19}$  GeV (Planck energy) and  $l^{-1} = 10^3$  GeV (TeV physics) are strong candidates. Another case is the cosmological model. Then we take  $\Lambda = 10^{19}$  GeV and  $l^{-1} = 10^{-41}$  GeV ([Cosmological Size]<sup>-1</sup>).  $\Lambda$  and  $l$  are huge numerical numbers when applied in the real world.

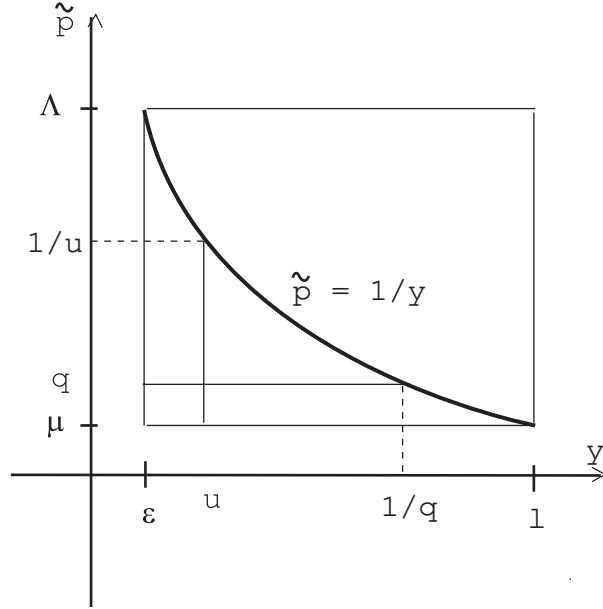


Fig. 1. Space of  $(y, \tilde{p})$  for integration. The hyperbolic curve will be used in Sec.5.

$$-\frac{e^{-(1-a)x}}{1-a} {}_2F_1\left(\frac{1-a}{2}, 1; \frac{3-a}{2}; e^{-2x}\right) - \frac{e^{-(1+a)x}}{1+a} {}_2F_1\left(\frac{1+a}{2}, 1; \frac{3+a}{2}; e^{-2x}\right),$$

$$x > 0, \quad 1 > a \geq 0, \quad (4.3)$$

where  ${}_2F_1(\alpha, \beta; \gamma; z)$  is Gauss's hypergeometric function. The formula below goes to the above one in the limit  $a \rightarrow 1 - 0$  (ignoring the divergent constant  $1/(a-1)$ ). The integrand of  $E_{Cas}(\Lambda, l)$  (4.2),  $\tilde{p}^3 F(\tilde{p}, y)$ , can be *exactly* evaluated as

$$\tilde{p}^3 F(\tilde{p}, y) = -\frac{\tilde{p}^3}{l} \left[ -\frac{3}{2} \frac{e^{-(1-a(y))x}}{1-a(y)} {}_2F_1\left(\frac{1-a(y)}{2}, 1; \frac{3-a(y)}{2}; e^{-2x}\right) - \frac{3}{2} \frac{e^{-(1+a(y))x}}{1+a(y)} {}_2F_1\left(\frac{1+a(y)}{2}, 1; \frac{3+a(y)}{2}; e^{-2x}\right) + \frac{5}{2} \ln \sinh(x) \right]_{x=\tilde{p}l}^{x=\Lambda l},$$

$$a(y) \equiv \left| 2\frac{y}{l} - 1 \right|, \quad \Lambda^{-1} \leq y < l, \quad l^{-1} \leq \tilde{p} \leq \Lambda. \quad (4.4)$$

Note that Eq.(4.2), with Eq.(4.4), is the *rigorous* expression of  $(\Lambda, l)$ -regularized Casimir energy. We show the behaviour of  $\tilde{p}^3 F(\tilde{p}, y)$  by taking the unit  $l = 1$  in Figs. 2-4. Three graphs correspond to  $\Lambda = 10, 100, \text{ and } 1000$ . All three graphs have a common shape. The behaviour along  $\tilde{p}$ -axis does not markedly depend on  $y$ . A valley 'runs' parallel to the  $y$ -axis with the bottom line at a fixed ratio of  $\tilde{p}/\Lambda \sim 0.75$ . \*) The depth of the valley is proportional to  $\Lambda^4$ . Because  $E_{Cas}$  is the  $(\tilde{p}, y)$  'flat-

\*) The valley-bottom line ('path')  $\tilde{p} = \tilde{p}(y) \approx 0.75\Lambda$  corresponds to the solution of the minimal

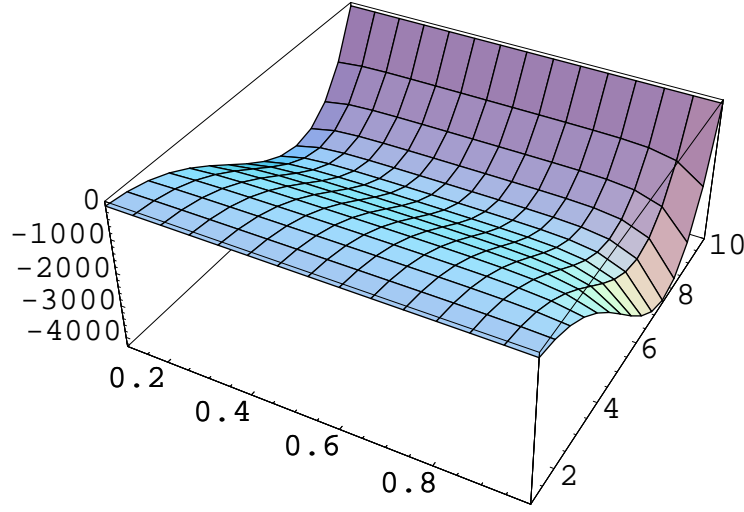


Fig. 2. Behaviour of  $\tilde{p}^3 F(\tilde{p}, y)$  (4.4).  $l = 1$ ,  $\Lambda = 10$ ,  $0.1 \leq y < 1$ ,  $1 \leq \tilde{p} \leq 10$ .

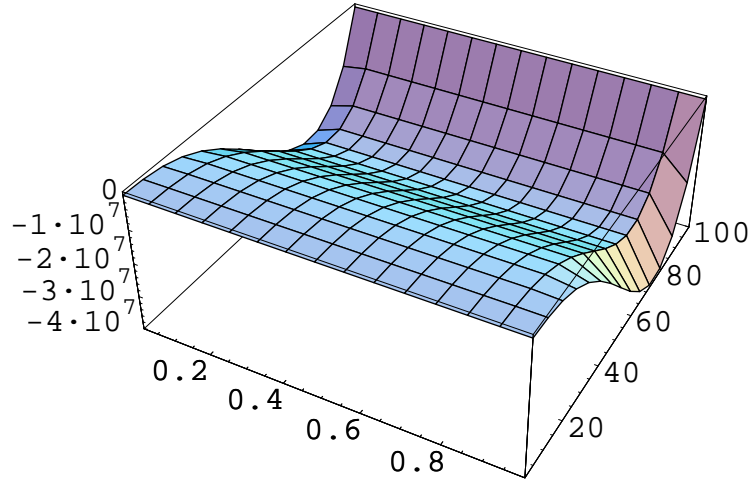


Fig. 3. Behaviour of  $\tilde{p}^3 F(\tilde{p}, y)$  (4.4).  $l = 1$ ,  $\Lambda = 100$ ,  $0.01 \leq y < 1$ ,  $1 \leq \tilde{p} \leq 100$ .

plane' integral of  $\tilde{p}^3 F(\tilde{p}, y)$ , the *volume* inside the valley is the quantity  $E_{Cas}$ . It is easy to see that  $E_{Cas}$  is proportional to  $\Lambda^5$ . This is consistent with Eq.(2.24). Importantly, Eq.(4.2) shows the *scaling* behaviour for large values of  $\Lambda$  and  $l$ . From a *close* numerical analysis of the  $(\tilde{p}, y)$ -integral Eq.(4.2), we confirm (see Appendix

'action' principle:  $\delta S = 0$ ,  $S \equiv (1/8\pi^2) \int d\tilde{p} \int dy \tilde{p}^3 F(\tilde{p}, y)$ . This will be referred to in §7.

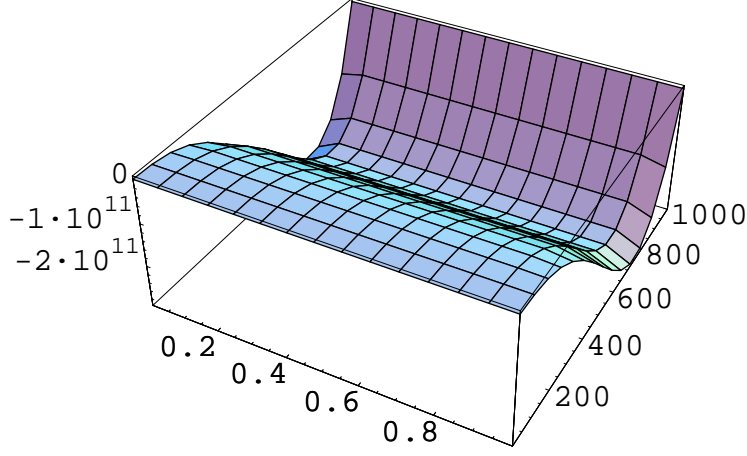


Fig. 4. Behaviour of  $\tilde{p}^3 F(\tilde{p}, y)$  (4.4).  $l = 1$ ,  $\Lambda = 1000$ ,  $0.001 \leq y < 1$ ,  $1 \leq \tilde{p} \leq 1000$ .

C) that

$$E_{Cas}(\Lambda, l) = \frac{2\pi^2}{(2\pi)^4} [-0.1249\Lambda^5 - (1.41, 0.706, 0.353) \times 10^{-5} \Lambda^5 \ln(\Lambda)] . \quad (4.5)$$

(Note:  $0.125 = (1/8) \times (1/5) \times (4[\text{even}] + 1[\text{odd}])$ .) This is the essentially the same result as that in §2. \*)

Finally we notice, from Figs. 2–4, that the approximate form of  $F(\tilde{p}, y)$  for large values of  $\Lambda$  and  $l$  is given by

$$F(\tilde{p}, y) \approx -\frac{f}{2}\Lambda \left(1 - \frac{\tilde{p}}{\Lambda}\right) , \quad f = 5 , \quad (4.6)$$

which does *not* depend on  $y$  or  $l$ . \*)  $f$  is the *degree of freedom*. From this result, we know, using the integral expression (3.22), that the following *approximate* form of the integrand of  $F^\mp$  is valid in a wide range  $(\tilde{k}, y)$ .

$$\text{Intgrd}F^\mp(\tilde{k}, y; l) \equiv \frac{\cosh \tilde{k}(2y - l) - \cosh \tilde{k}l}{2 \sinh(\tilde{k}l)} \approx -\frac{1}{2} ,$$

---

\*) Note that the result of Eq.(2.24) in Sec.2 is obtained from the KK-expanded form, whereas that of Eq.(4.5) in this section from the *closed* expression. The coincidence ( $\Lambda^5$  proportionality) strongly shows the correctness of both evaluations. At the same time, the numerical result for the first term coefficient shows that the number of significant figures is 4. Although the second term contribution is small, its coefficient is not stable and its significant digits is 1 at most. The triplet data correspond to  $l = 10, 20$  and  $40$ .

\*) Using the approximate form Eq.(4.6),  $E_{Cas}$  is estimated as  $E_{Cas}(\Lambda, l) \times 8\pi^2 \approx \int_{1/l}^{\Lambda} d\tilde{p} \int_{1/\Lambda}^l dy \tilde{p}^3 (-5/2)(\Lambda - \tilde{p}) = -(1/8)\Lambda^5 (1 + O(1/\Lambda))$ . This is consistent with Eq.(4.5).

$$\text{Intgrd}F^+(\tilde{k}, y; l) \equiv \frac{-\cosh \tilde{k}(2y - l) - \cosh \tilde{k}l}{2 \sinh(\tilde{k}l)} \approx -\frac{1}{2} \quad ,$$

$$(\tilde{k}, y) \in \{(\tilde{k}, y) | \tilde{k}y \gg 1 \text{ and } \tilde{k}(l - y) \gg 1\} \quad (4.7)$$

which can be analytically proved and is confirmed by graphically showing the above functions (see Figs.5 and 6. The table shape of the graphs implies the ‘‘Rayleigh-Jeans’’ dominance because Casimir energy density is proportional to the cubic power of  $\tilde{p}$  in the region  $\tilde{p} \ll \Lambda$ . \*\*)

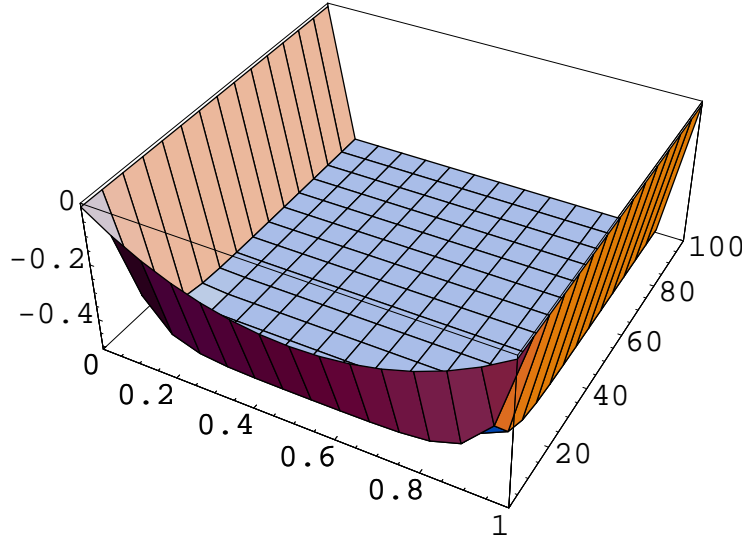


Fig. 5. Behaviour of the integrand of  $F^-$ ,  $\text{Intgrd}F^-(\tilde{k}, y; l)$  (4.7).  $l = 1$ ,  $\Lambda = 100$ ,  $0 \leq y \leq l = 1$ ,  $1 \leq \tilde{k} \leq \Lambda = 100$ . The flat plane locates at a height of  $-0.5$ .

## §5. UV and IR regularization surfaces, principle of minimal area and renormalization flow

We have confirmed that heat-kernel formulation is equivalent to the familiar KK-expansion approach. The advantage of the new approach is that the KK expansion is replaced by the integral over the extradimensional coordinate  $y$  and all expressions are written in the closed (not expanded) form. The  $\Lambda^5$ -divergence shows notorious problem of higher dimensional theories. In spite of all previous studies, we have not succeeded in defining higher-dimensional theories. (In this free theory case, the divergence is simple and the *finite* Casimir energy (force) can be read as shown in

\*\*) The well-known radiation spectral formula ( $\beta$  is the inverse temperature):  $\langle E \rangle_{\nu, \beta} = h\nu/2 + h\nu/(e^{\beta h\nu} - 1)$  consists of two parts. The first one is the zero-point energy and the second is Planck's distribution part. The low-frequency region of Planck's distribution formula:  $h\nu/(e^{\beta h\nu} - 1) \approx 1/\beta$  (independent of  $\nu$ ),  $h\nu \ll 1/\beta$ , is called Rayleigh-Jeans region. Note that the extra coordinate  $y$  or  $l - y$ , in the present 5D model, plays the role of the inverse temperature  $\beta$ .

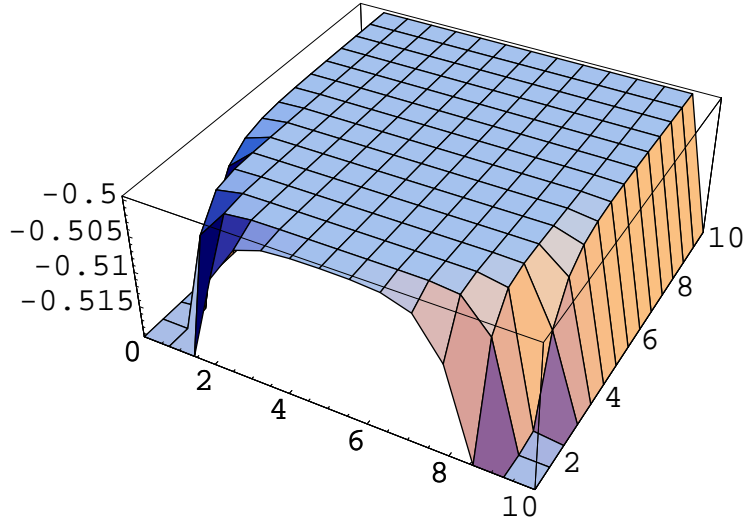


Fig. 6. Behaviour of the integrand of  $F^+$ ,  $\text{Intgrd}F^+(\tilde{k}, y; l)$  (4.7).  $l = 10$ ,  $\Lambda = 10$ ,  $0 \leq y \leq l = 10$ ,  $1 \leq \tilde{k} \leq \Lambda = 10$ . The flat plane locates at a height of  $-0.5$ .

Eq.(2.25). In general, however, the divergences cause problems. The famous example is the divergent *cosmological constant* in the gravity-involving theories.<sup>3)</sup> We notice here that we can solve the divergence problem if we find a way to *legitimately restrict the integral region in  $(\tilde{p}, y)$ -space*.

One proposal of this was presented by Randall and Schwartz.<sup>9)</sup> They introduced the *position-dependent cutoff*,  $\mu < \tilde{p} < 1/u$ , and  $u \in [\epsilon, l]$ , for the 4D-momentum integral in the “brane” located at  $y = u$ . (See Fig. 1.) The total integral region is the lower part of the hyperbolic curve  $\tilde{p} = 1/y$ . They succeeded in obtaining the *finite  $\beta$ -function* in the 5D warped vector model. We have confirmed that the  $E_{Cas}$  obtained using Eq.(4.2), when the Randall-Schwartz integral region (Fig. 1) is taken, is proportional to  $\Lambda^4$ . A close numerical analysis shows (see Appendix C)

$$\begin{aligned} E_{Cas}^{RS} &= \frac{2\pi^2}{(2\pi)^4} \int_{1/l}^{\Lambda} dq \int_{1/\Lambda}^{1/q} dy q^3 F(q, y) = \frac{2\pi^2}{(2\pi)^4} \int_{1/\Lambda}^l du \int_{1/l}^{1/u} d\tilde{p} \tilde{p}^3 F(\tilde{p}, u) \\ &= \frac{2\pi^2}{(2\pi)^4} [-8.93814 \times 10^{-2} \Lambda^4] \quad , (5.1) \end{aligned}$$

which is *independent* of  $l$ . \*) This shows that the divergence situation is indeed improved compared with the  $\Lambda^5$ -divergence of Eq.(4.5).

Although Randall and Schwartz claim that holography (for the case of the warped geometry) is behind the procedure, the legitimacy of the restriction looks

\*) The result of Eq.(5.1) is consistent with the approximate form of  $F$  obtained in Eq.(4.6).  $(-5/2) \int_{1/l}^{\Lambda} dq \int_{1/\Lambda}^{1/q} dy q^3 (\Lambda - q) = -(1/12)\Lambda^4 (1 + O(1/(\Lambda l)^3))$ .  $0.0893 \approx 0.0833 \dots = 1/12$ .



less obvious. We have proposed an alternative approach and given a legitimate explanation within the 5D QFT.<sup>10),25),26)</sup> Here we closely examine the new regularization.

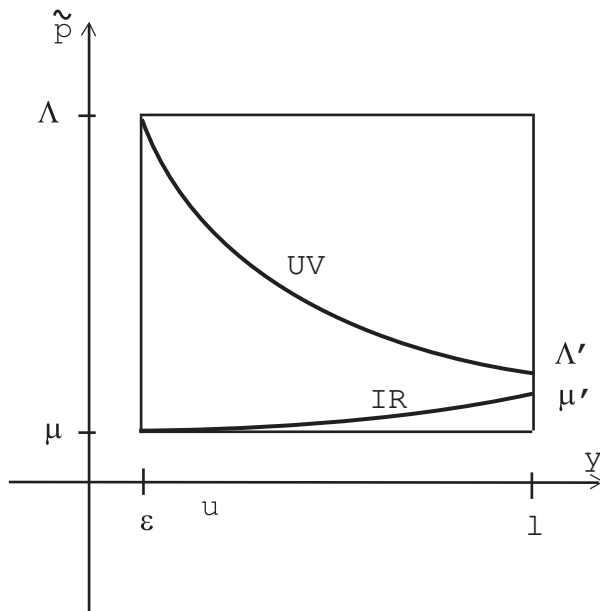


Fig. 7. Space of  $(\tilde{p}, y)$  for the integration (present proposal).

On the “3-brane” at  $y = \epsilon$ , we introduce the IR cutoff  $\mu$  and the UV cutoff  $\Lambda$  ( $\mu \ll \Lambda$ ) (see Fig.7),

$$\mu \ll \Lambda \quad . \quad (5.2)$$

This is legitimate in the sense that we generally perform this procedure in 4D *renormalizable* theories. (Here we are considering those 5D theories that are renormalizable in 3-branes. Examples are 5D electromagnetism (the present model), the 5D  $\Phi^4$ -theory, and the 5D Yang-Mills theory.) For the same reason, on the “3-brane” at  $y = l$ , we may have another set of IR and UV cutoffs,  $\mu'$  and  $\Lambda'$ . We consider the case,

$$\mu' \leq \Lambda', \quad \Lambda' \ll \Lambda, \quad \mu \sim \mu' \quad . \quad (5.3)$$

This case will enable us to introduce *renormalization flow*, (see our later discussion.) We claim here that, as for the “3-brane” located at each point  $y$  ( $\epsilon < y < l$ ), the regularization parameters are determined by the *minimal area principle*.<sup>\*)</sup> To explain this, we move to the 5D coordinate space  $(x^\mu, y)$ , (see Fig. 8). The  $\tilde{p}$ -expression is replaced with the  $\sqrt{x_\mu x^\mu}$ -expression by *reciprocal relation*,

$$\sqrt{x_\mu(y)x^\mu(y)} \equiv r(y) \quad \leftrightarrow \quad \frac{1}{\tilde{p}(y)} \quad . \quad (5.4)$$

<sup>\*)</sup> We do *not* quantize the (bulk) geometry, but treat it as the *background*. The (bulk) geometry fixes the behavior of the *regularization* cutoff parameters in the field quantization. The geometry influences the “boundary” of the field-quantization procedure in this way.

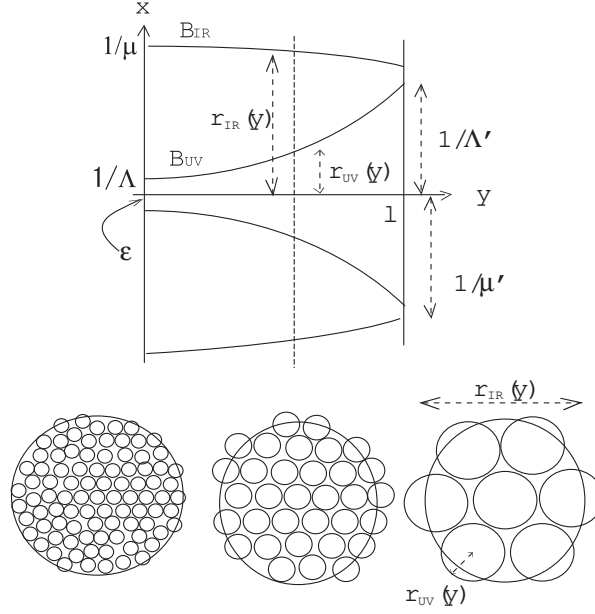


Fig. 8. Regularization surfaces  $B_{IR}$  and  $B_{UV}$  in the 5D coordinate space  $(x^\mu, y)$ , flow of coarse graining (renormalization) and sphere lattice regularization.

The UV and IR cutoffs change along the  $y$ -axis and the trajectories form *surfaces* in the 5D bulk space  $(x^\mu, y)$ . We *require* that the two surfaces do *not* cross for the purpose of the renormalization group interpretation (discussed later). We call them UV and IR regularization (or boundary) surfaces ( $B_{UV}$  and  $B_{IR}$ ),

$$\begin{aligned} B_{UV} & : \quad \sqrt{(x^1)^2 + (x^2)^2 + (x^3)^2 + (x^4)^2} = r_{UV}(y) \quad , \quad \epsilon = \frac{1}{\Lambda} < y < l \quad , \\ B_{IR} & : \quad \sqrt{(x^1)^2 + (x^2)^2 + (x^3)^2 + (x^4)^2} = r_{IR}(y) \quad , \quad \epsilon = \frac{1}{\Lambda} < y < l \quad , \end{aligned} \quad (5.5)$$

The cross sections of the regularization surfaces at  $y$  are the spheres  $S^3$  with the radii  $r_{UV}(y)$  and  $r_{IR}(y)$ . Here, we consider the Euclidean space for simplicity. The UV-surface is stereographically shown in Fig. 9 and reminds us of the *closed string* propagation. Note that the boundary surface  $B_{UV}$  (and  $B_{IR}$ ) is the four-dimensional manifold.

The 5D volume region bounded by  $B_{UV}$  and  $B_{IR}$  is the integral region of Casimir energy  $E_{Cas}$ . The forms of  $r_{UV}(y)$  and  $r_{IR}(y)$  can be determined by the *minimal area principle*,

$$\delta(\text{Surface Area}) = 0 \quad , \quad 3 - \frac{r \frac{d^2 r}{dy^2}}{1 + (\frac{dr}{dy})^2} = 0 \quad , \quad 0 \leq y \leq l \quad . \quad (5.6)$$

In Appendix A, we present the classification of all solutions (paths) and the general analytic solution. In Fig. 10, we show two result curves of Eq.(5.6), taking the boundary conditions ( $r' \equiv dr/dy$ ):

Fig. 10: Fine configuration goes to coarse configuration as  $y$  increases

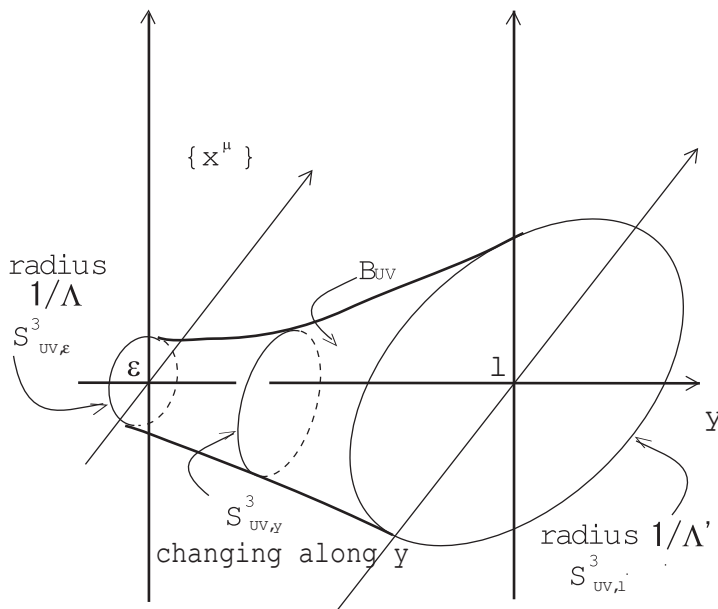


Fig. 9. UV regularization surface in 5D coordinate space.

$$\begin{aligned}
 \text{IR curve (upper):} & \quad r[0] = 12.0, r'[0] = -1.0 \quad [\text{simply decreasing type}], \\
 \text{UV curve (lower):} & \quad r[1.0] = 10.0, r'[1.0] = 350.0 \quad [\text{simply-increasing type}].
 \end{aligned} \tag{5.7}$$

where the types of curves are specified on the basis of the classification of the minimal surface lines in App. A1. They show that the renormalization flow shown in Fig. 7 really occurs by the minimal area principle. In Fig. 11, another set of minimal surface lines are given by taking another boundary conditions.

Fig. 11: Coarse Conf. goes to Fine Conf. as  $y$  increases

$$\begin{aligned}
 \text{IR curve (upper):} & \quad r[0] = 4.6, r'[0] = -1.0 \quad [\text{simply decreasing type}] \quad , \\
 \text{UV curve (lower):} & \quad r[0] = 4.5, r'[0] = -22.0 \quad [\text{simply decreasing type}] \quad .
 \end{aligned} \tag{5.8}$$

They show the opposite-direction flow of renormalization compared with that in Fig. 10. (See the next paragraph for the renormalization flow interpretation.) These two examples imply that the *boundary conditions* determine the property of the renormalization flow. \*)

The present regularization scheme also gives the *renormalization group* interpretation of the change in physical quantities along the extra axis (see Fig. 8). \*\*) In

\*) The minimal area equation Eq.(5.6) is the second-derivative differential equation and has the general solution (see Appendix A). Hence, for the given two initial conditions (for example,  $r(y = \epsilon)$  and  $dr/dy|_{y=\epsilon}$ ), there exists a unique analytic solution. The presented graphs are those with these initial conditions. Another choice of the initial conditions,  $r(y = \epsilon)$  and  $r(y = l)$ , is possible. Generally, the solution of the second-derivative differential equation is fixed by two *boundary conditions*.

\*\*) This part is in contrast to the AdS/CFT approach where the renormalization flow comes from the Einstein equation of 5D supergravity.

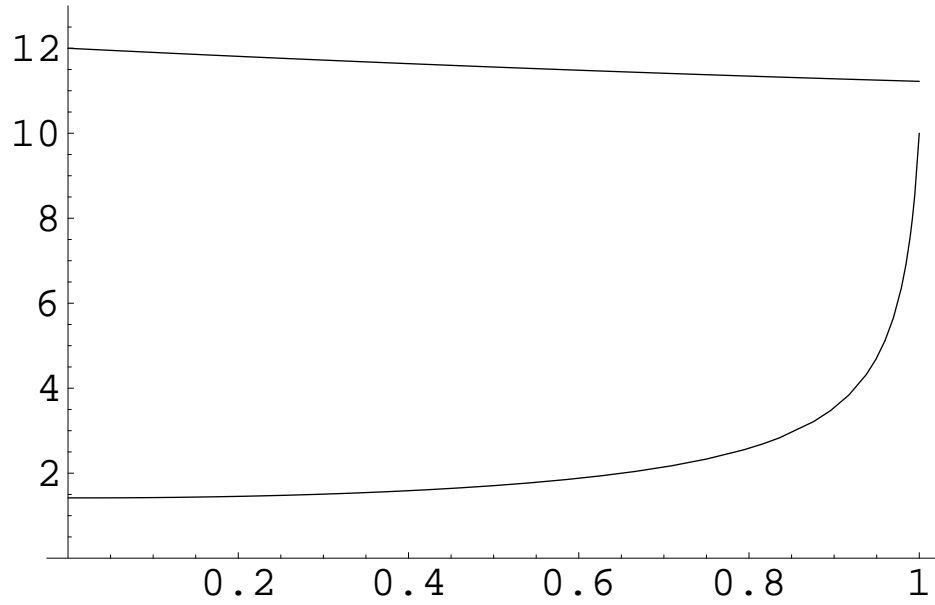


Fig. 10. Numerical solution of Eq.(5-6). Vertical axis:  $r$ ; horizontal axis:  $0 \leq y \leq l = 1$ . IR curve (upper):  $r[0] = 12.0$ ,  $r'[0] = -1.0$  [simply decreasing type]; UV curve (lower):  $r[1.0] = 10.0$ ,  $r'[1.0] = 350.0$  [simply increasing type].

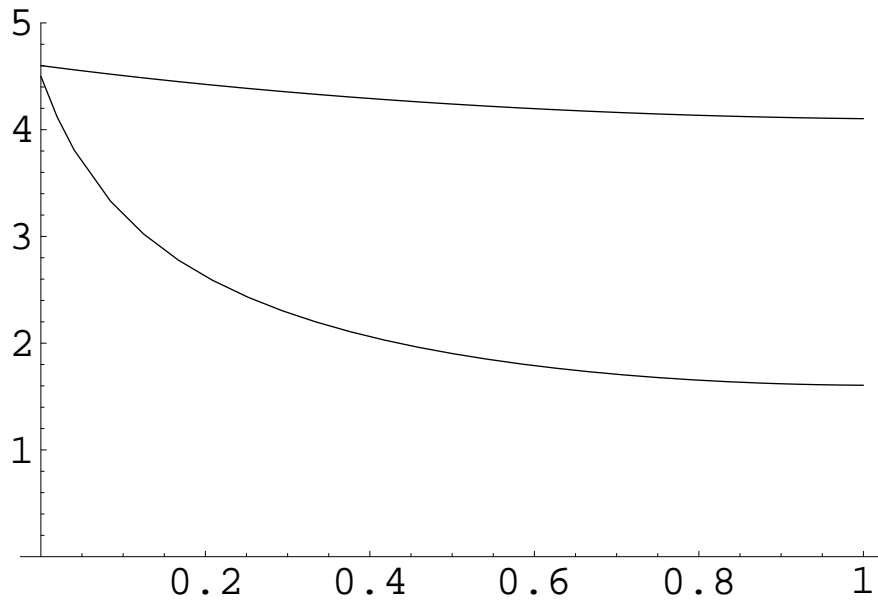


Fig. 11. Numerical solution of (5-6). Vertical axis:  $r$ ; Horizontal axis:  $0 \leq y \leq l = 1$ . IR curve (upper):  $r[0] = 4.6$ ,  $r'[0] = -1.0$  [simply decreasing type]; UV curve (lower):  $r[0] = 4.5$ ,  $r'[0] = -22.0$  [simply decreasing type].

the “3-brane” located at  $y$ , the UV cutoff is  $r_{UV}(y)$  and the regularization surface is the sphere  $S^3$  with the radius  $r_{UV}(y)$ . The IR cutoff is  $r_{IR}(y)$  and the regularization surface is another sphere  $S^3$  with a radius  $r_{IR}(y)$ . We can regard the regularization integral region as the *sphere lattice* of the following properties:

Unit lattice (cell): the sphere  $S^3$  with radius  $r_{UV}(y)$  and its inside,

Total lattice: the sphere  $S^3$  with radius  $r_{IR}(y)$  and its inside.

It is composed of many cells above,

$$\text{Total number of cells: } \text{const} \times \left( \frac{r_{IR}(y)}{r_{UV}(y)} \right)^4 . \quad (5-9)$$

The total number of cells changes from  $(\frac{\Delta}{\mu})^4$  at  $y = \epsilon$  to  $(\frac{\Delta'}{\mu'})^4$  at  $y = l$ . Along the  $y$ -axis, the number increases as

$$\left( \frac{r_{IR}(y)}{r_{UV}(y)} \right)^4 \equiv N(y) . \quad (5-10)$$

For the “scale” change  $y \rightarrow y + \Delta y$ ,  $N$  changes as

$$\Delta(\ln N) = 4 \frac{\partial}{\partial y} \left\{ \ln \left( \frac{r_{IR}(y)}{r_{UV}(y)} \right) \right\} \cdot \Delta y . \quad (5-11)$$

When the system has some coupling  $g(y)$ , the renormalization group  $\beta(g)$  function (along the extra axis) is expressed as

$$\beta = \frac{\Delta(\ln g)}{\Delta(\ln N)} = \frac{1}{\Delta(\ln N)} \frac{\Delta g}{g} = \frac{1}{4} \frac{1}{\frac{\partial}{\partial y} \ln \left( \frac{r_{IR}(y)}{r_{UV}(y)} \right)} \frac{1}{g} \frac{\partial g}{\partial y} , \quad (5-12)$$

where  $g(y)$  is the renormalized coupling at  $y$ . \*)

We have confirmed that the minimal area principle determines the flow of the regularization surfaces. Among the numerical results, some curves are similar to the type proposed by Randall-Schwartz.

## §6. Weight function and Casimir energy evaluation

In Eq.(3-22), Casimir energy is written by the integral in the  $(\tilde{p}, y)$  space in the range:  $0 \leq y \leq l$  and  $0 \leq \tilde{p} \leq \infty$ . In § 5, we see that *the integral region should be properly restricted* because the cutoff region in the 4D world changes along the extra axis obeying the bulk (flat) geometry (minimal area principle). In this section, we consider an alternative version.

Instead of restricting the integral region, we introduce the *weight function*  $W(\tilde{p}, y)$  in the  $(\tilde{p}, y)$ -space to suppress the UV and IR divergences of Casimir energy.

$$E_{Cas}^W(l) \equiv \int \frac{d^4 p}{(2\pi)^4} \int_0^l dy W(\tilde{p}, y) F(\tilde{p}, y), \quad F(\tilde{p}, y) \equiv F^-(\tilde{p}, y) + 4F^+(\tilde{p}, y) ,$$

---

\*) Here we consider interacting theories, such as the 5D Yang-Mills theory and 5D  $\Phi^4$  theory, where the coupling  $g(y)$  is the renormalized one in the ‘3-brane’ at  $y$ .

Examples of  $W(\tilde{p}, y)$  :  $W(\tilde{p}, y) =$

$$\left\{ \begin{array}{ll} \frac{1}{N_1} e^{-(1/2)l^2\tilde{p}^2 - (1/2)y^2/l^2} \equiv W_1(\tilde{p}, y), & N_1 = \frac{1.557}{8\pi^2} \quad \text{elliptic sup.,} \\ \frac{1}{N_{1b}} e^{-(1/2)l^2\tilde{p}^2} \equiv W_{1b}(\tilde{p}, y), & N_{1b} = \frac{1.820}{8\pi^2} \quad \text{kinetic-energy sup.,} \\ \frac{1}{N_2} e^{-\tilde{p}y} \equiv W_2(\tilde{p}, y), & N_2 = \frac{2(l\Lambda)^3}{8\pi^2} \quad \text{hyperbolic sup. 1,} \\ \frac{1}{N_3} e^{-(1/2)\tilde{p}^2 y^2} \equiv W_3(\tilde{p}, y), & N_3 = \frac{2}{3} \frac{(l\Lambda)^3}{8\pi^2} \quad \text{hyperbolic sup. 2,} \\ \frac{1}{N_4} e^{-(1/2)l^4\tilde{p}^2/y^2} \equiv W_4(\tilde{p}, y), & N_4 = \frac{0.3222}{8\pi^2} \quad \text{linear sup.,} \\ \frac{1}{N_5} e^{-l^3\tilde{p}/y^2} \equiv W_5(\tilde{p}, y), & N_5 = \frac{0.6342}{8\pi^2} \quad \text{parabolic sup. 1,} \\ \frac{1}{N_6} e^{-l^3\tilde{p}^2/y} \equiv W_6(\tilde{p}, y), & N_6 = \frac{0.09788}{8\pi^2} \quad \text{parabolic sup. 2,} \\ \frac{1}{N_7} e^{-(1/2)l^4\tilde{p}^4} \equiv W_7(\tilde{p}, y), & N_7 = \frac{0.3033}{8\pi^2} \quad \text{higher-derivative sup. 1,} \\ \frac{1}{N_8} e^{-(l^2/2)(\tilde{p}^2+1/y^2)} \equiv W_8(\tilde{p}, y), & N_8 = \frac{0.3800}{8\pi^2} \quad \text{reciprocal sup. 1,} \\ \frac{1}{N_{47}} e^{-(l^4/2)\tilde{p}^2(\tilde{p}^2+1/y^2)} \equiv W_{47}(\tilde{p}, y), & N_{47} = \frac{0.03893}{8\pi^2} \quad \text{higher-derivative sup. 2,} \\ \frac{1}{N_{56}} e^{-(l^3/2)(\tilde{p}/y)(\tilde{p}+1/y)} \equiv W_{56}(\tilde{p}, y), & N_{56} = \frac{0.1346}{8\pi^2} \quad \text{reciprocal sup. 2,} \\ \frac{1}{N_{88}} e^{-(l^4/2)(\tilde{p}^2+1/y^2)^2} \equiv W_{88}(\tilde{p}, y), & N_{88} = \frac{0.005006}{8\pi^2} \quad \text{higher-der reciprocal sup.,} \\ \frac{1}{N_9} e^{-(l^2/2)(\tilde{p}+1/y)^2} \equiv W_9(\tilde{p}, y), & N_9 = \frac{0.03921}{8\pi^2} \quad \text{reciprocal sup. 3.} \end{array} \right. \quad (6\cdot 1)$$

where  $F^\mp$  are defined in Eq.(3\cdot 22) and  $N_i$  are the normalization constants. \*) \*\*) Above, we list some examples expected for the weight function  $W(\tilde{p}, y)$ .  $W_2$  and  $W_3$  are considered to correspond to the regularization taken by Randall-Schwartz. How to specify the form of  $W$  is the subject of the next section. We show the shape of the

\*) In the flat geometry, the periodicity parameter  $l$  is a unique scale parameter. We make all exponents in Eq.(6\cdot 1) dimensionless using  $l$ .

\*\*) The normalization constants  $N_i$  are defined by

$$\int_{l^{-1} < \tilde{p} < \Lambda} \frac{d^4 p}{(2\pi)^4} \int_{\Lambda^{-1}}^l dy W_i(\tilde{p}, y) = \frac{1}{8\pi^2} \frac{1}{l^3} \int_1^{l\Lambda} dx \int_{(l\Lambda)^{-1}}^1 dw x^3 W_i\left(\frac{x}{l}, lw\right) = \frac{1}{l^3} \quad , \quad l\Lambda \gg 1 \quad (6\cdot 2)$$

where  $x \equiv l\tilde{p}$  and  $w \equiv y/l$ . They are explicitly given by

$$\begin{aligned} 8\pi^2 N_1 &= \frac{3}{\sqrt{e}} \int_0^1 dw e^{-w^2/2} = 1.557 \quad , \quad 8\pi^2 N_{1b} = \frac{3}{\sqrt{e}} = \int_1^\infty dx x^3 e^{-x^2/2} = 1.820 \quad , \\ 8\pi^2 N_2 &= \int_1^\infty dx \int_{(l\Lambda)^{-1}}^1 dw x^3 e^{-xw} = 2(l\Lambda)^3 \quad , \quad 8\pi^2 N_3 = \int_1^\infty dx \int_{(l\Lambda)^{-1}}^1 dw x^3 e^{-x^2 w^2/2} = (2/3)(l\Lambda)^3 \quad , \\ 8\pi^2 N_4 &= \int_1^\infty dx \int_0^1 dw x^3 e^{-x^2/2w^2} = 0.3222 \quad , \quad 8\pi^2 N_5 = \int_1^\infty dx \int_0^1 dw x^3 e^{-x/w^2} = 0.6342 \quad , \\ 8\pi^2 N_6 &= \int_1^\infty dx \int_0^1 dw x^3 e^{-x^2/w} = 0.09788 \quad , \quad 8\pi^2 N_7 = \int_1^\infty dx x^3 e^{-x^4/2} = \frac{1}{2\sqrt{e}} = 0.3033 \quad , \\ 8\pi^2 N_8 &= \frac{3}{\sqrt{e}} \int_0^1 dw e^{-1/2w^2} = 0.3800 \quad , \quad 8\pi^2 N_{47} = \int_1^\infty dx \int_0^1 dw x^3 e^{-x^2(x^2+1/w^2)/2} = 0.03893 \quad , \\ & \quad 8\pi^2 N_{56} = \int_1^\infty dx \int_0^1 dw x^3 e^{-(x/w)(x+1/w)/2} = 0.1346 \quad , \\ & \quad 8\pi^2 N_{88} = \int_1^\infty dx \int_0^1 dw x^3 e^{-(1/2)(x^2+1/w^2)^2} = 0.005006 \quad , \\ & \quad 8\pi^2 N_9 = \int_1^\infty dx \int_0^1 dw x^3 e^{-(1/2)(x+1/w)^2} = 0.03921 \quad .(6\cdot 3) \end{aligned}$$

energy integrand  $\tilde{p}^3 W(\tilde{p}, y) F(\tilde{p}, y)$  in Figs. 12–15. We notice that the valley-bottom line  $\tilde{p} \approx 0.75\Lambda$ , which appeared in the unweighted case (Figs. 2–4), is replaced by new lines:  $\tilde{p} \approx \text{const}$  (Fig. 12,  $W_1$ ),  $\tilde{p}y \approx \text{const}$  (Fig. 13,  $W_3$ ),  $\tilde{p} \approx \text{const} \times y$  (Fig. 14,  $W_4$ ),  $\tilde{p} \approx \text{const} \times \sqrt{y}$  (Fig. 15,  $W_6$ ). They are all located away from the original  $\Lambda$ -effected line:  $\tilde{p} \sim 0.75\Lambda$ .

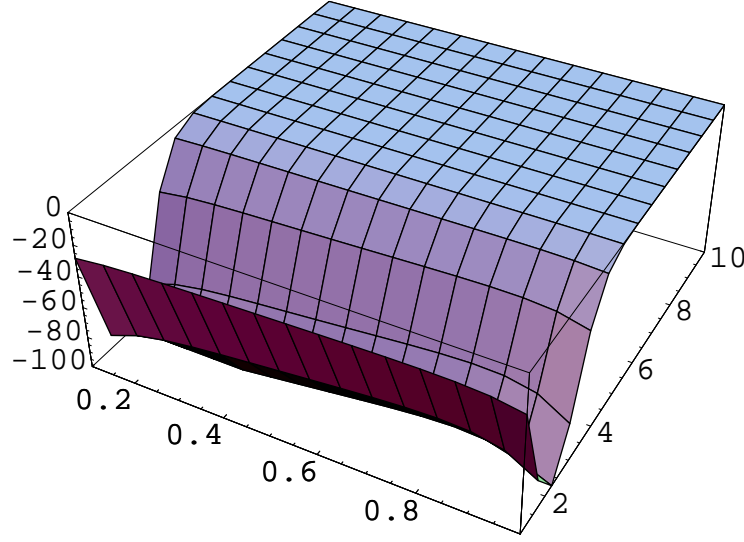


Fig. 12. Behaviour of  $\tilde{p}^3 W_1(\tilde{p}, y) F(\tilde{p}, y)$  (elliptic suppression).  $\Lambda = 10$ ,  $l = 1$ ,  $1/\Lambda \leq y \leq 0.99999l$ ,  $1/l \leq \tilde{p} \leq \Lambda$ .

We can check the divergence (scaling) behaviour of  $E_{Cas}^W$  by numerically evaluating the  $(\tilde{p}, y)$ -integral (6.1) for the rectangle region of Fig. 1. \*)

$$E_{Cas}^W =$$

---

\*) See Appendix C for the explanation of the numerical derivation.

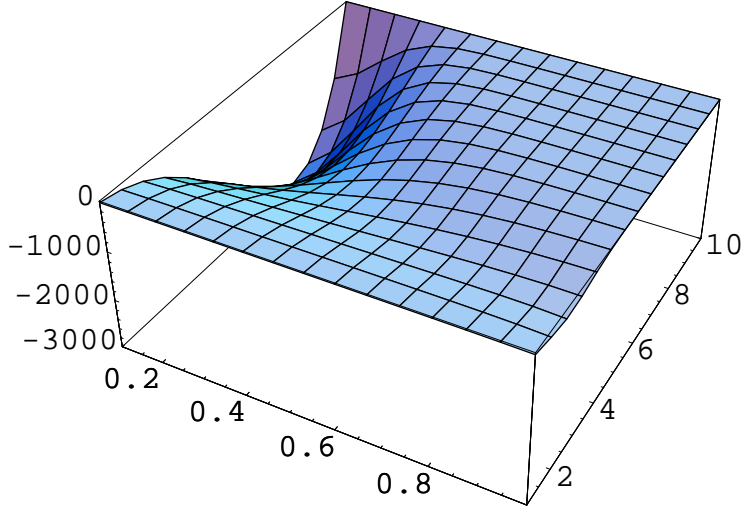


Fig. 13. Behaviour of  $\tilde{p}^3 W_3(\tilde{p}, y) F(\tilde{p}, y)$  (hyperbolic suppression 2).  $\Lambda = 10$ ,  $l = 1$ ,  $1/\Lambda \leq y \leq 0.99999l$ ,  $1/l \leq \tilde{p} \leq \Lambda$ .

$$\left\{ \begin{array}{ll}
 - (2.500, 2.501, 2.501) \frac{\Lambda}{l^3} + (-0.142, 1.09, 1.13) \times 10^{-4} \frac{\Lambda \ln(\Lambda)}{l^3} & \text{for } W_1, \\
 - (2.502, 2.502, 2.502) \frac{\Lambda}{l^3} + (2.40, 2.44, 1.84) \times 10^{-4} \frac{\Lambda \ln(\Lambda)}{l^3} & \text{for } W_{1b}, \\
 - (6.0392, 6.0394, 6.03945) \times 10^{-2} \frac{\Lambda}{l^3} & \\
 \quad - (24.7, 2.79, 1.60) \times 10^{-8} \frac{\Lambda \ln(\Lambda)}{l^3} & \text{for } W_2, \\
 - (10.650, 9.21917, 9.21915) \times 10^{-2} \frac{\Lambda}{l^3} & \\
 \quad + (153.3, 1.9629624, 1.9629620) \times 10^{-5} \frac{\Lambda \ln(\Lambda)}{l^3} & \text{for } W_3, \\
 - (2.55, 2.53, 2.52) \frac{\Lambda}{l^3} + (4.56, 2.63, 1.48) \times 10^{-3} \frac{\Lambda \ln(\Lambda)}{l^3} & \text{for } W_4, \\
 - (2.55, 2.54, 2.52) \frac{\Lambda}{l^3} + (6.10, 3.63, 2.10) \times 10^{-3} \frac{\Lambda \ln(\Lambda)}{l^3} & \text{for } W_5, \quad (6.4) \\
 - (2.532, 2.519, 2.511) \frac{\Lambda}{l^3} + (3.19, 1.83, 1.03) \times 10^{-3} \frac{\Lambda \ln(\Lambda)}{l^3} & \text{for } W_6, \\
 - (2.51, 2.51, 2.50) \frac{\Lambda}{l^3} + (8.51, 5.51, 3.36) \times 10^{-4} \frac{\Lambda \ln(\Lambda)}{l^3} & \text{for } W_7, \\
 - (2.52, 2.51, 2.51) \frac{\Lambda}{l^3} + (19.5, 11.6, 6.68) \times 10^{-4} \frac{\Lambda \ln(\Lambda)}{l^3} & \text{for } W_8, \\
 - (2.55, 2.55, 2.55) \frac{\Lambda}{l^3} + (5.47, 5.32, 5.01) \times 10^{-3} \frac{\Lambda \ln(\Lambda)}{l^3} & \text{for } W_{47}, \\
 - (2.54, 2.53, 2.52) \frac{\Lambda}{l^3} + (4.30, 2.48, 1.40) \times 10^{-3} \frac{\Lambda \ln(\Lambda)}{l^3} & \text{for } W_{56}, \\
 - (2.61, 2.61, 2.60) \frac{\Lambda}{l^3} + (1.20, 1.17, 1.10) \times 10^{-2} \frac{\Lambda \ln(\Lambda)}{l^3} & \text{for } W_{88}, \\
 - (2.54, 2.52, 2.51) \frac{\Lambda}{l^3} + (3.75, 2.16, 1.22) \times 10^{-3} \frac{\Lambda \ln(\Lambda)}{l^3} & \text{for } W_9.
 \end{array} \right.$$

The above fitting is obtained by taking the data for the range:  $l = (10, 20, 40)$ ,  $\Lambda = 10 \sim 10^3$ . The round-bracketed triplet data, corresponding to three values of  $l$ , should be the same if the scaling region is properly examined. The small fluctuation in the last digit number tells us the significant figures. The leading terms (linearly divergent terms) are firmly obtained, and the number of the significant figures (NSF)



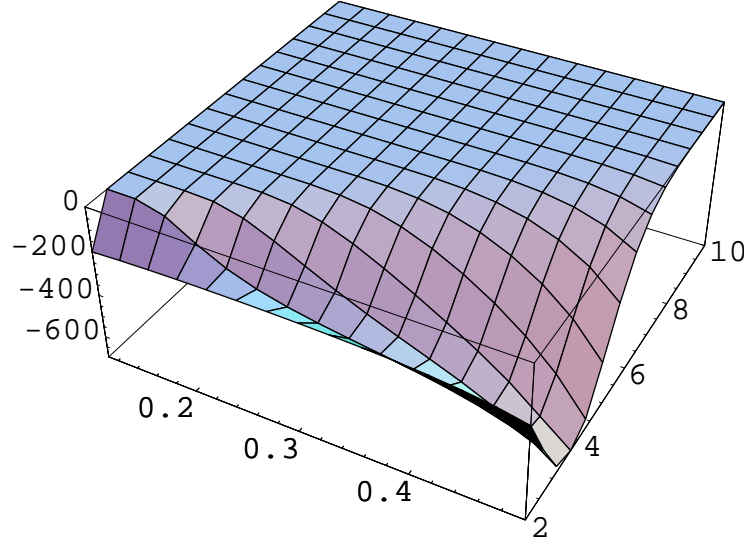


Fig. 14. Behaviour of  $\tilde{p}^3 W_4(\tilde{p}, y) F(\tilde{p}, y)$  (linear suppression).  $\Lambda = 10$ ,  $l = 0.5$ ,  $1/\Lambda \leq y \leq 0.99999l$ ,  $1/l \leq \tilde{p} \leq \Lambda$ .

$\geq 3$ . The log terms are obtained very poorly, and the NSF is 1 at best. <sup>\*)</sup> The divergent normalization constants of  $W_2$  and  $W_3$ , namely,  $N_2$  and  $N_3$ , are consistent with Eq.(5.1). <sup>\*\*)</sup> After normalizing the factor  $\Lambda l$ , *only the log-divergence* remains.

$$E_{Cas}^W / \Lambda l = -\frac{\alpha}{l^4} (1 - 4c \ln(l\Lambda)) \quad , \quad (6.5)$$

where  $\alpha$  can be read from Eq.(6.4). (For the 5D EM (2.24),  $\alpha$  corresponds to the value  $5 \times 3\zeta(5)/(4 \times 8\pi^2) \approx 3.86/8\pi^2$ .) The numerical results say that  $\alpha$  does not so much depend on the choice of  $W$  except  $W_2$  and  $W_3$ . As for  $c$ , we expect that it reaches a fixed value as  $l$  increases further. Although the present approach leaves the weight function  $W(\tilde{p}, y)$  unspecified, and the numerical results involve some ambiguity, we can say that  $\alpha$  is approximately +2.5 (a positive number on the order of  $O(1)$ ), and  $c$  is a positive number on the order of  $O(10^{-4})$  to  $O(10^{-3})$ . (The hyperbolic cases,  $W_2$  and  $W_3$ , are exceptions. This is due to the divergent normalization factors  $N_2$  and  $N_3$  shown in Eq.(6.1)). At present, we cannot discriminate which weight is the right one. Here, we list the characteristic features (advantageous (Yes) or disadvantageous (No), independent (I) or dependent (D), and singular (S) or regular (R)) for each weight from the following points.

**point 1** The behavior of  $W$  for the limit  $l \rightarrow 0$  or  $l \rightarrow \infty$ . This property is related to the continuity to the ordinary field quantization.

**point 2** The path (bottom line of the valley) is independent (I) of the scale  $l$  or

<sup>\*)</sup> No data instability appears in a warped case.<sup>26)–28)</sup>

<sup>\*\*)</sup> In particular,  $W_2$  case is more similar to that in Eq.(5.1) in that the log term vanishes in the present numerical precision.

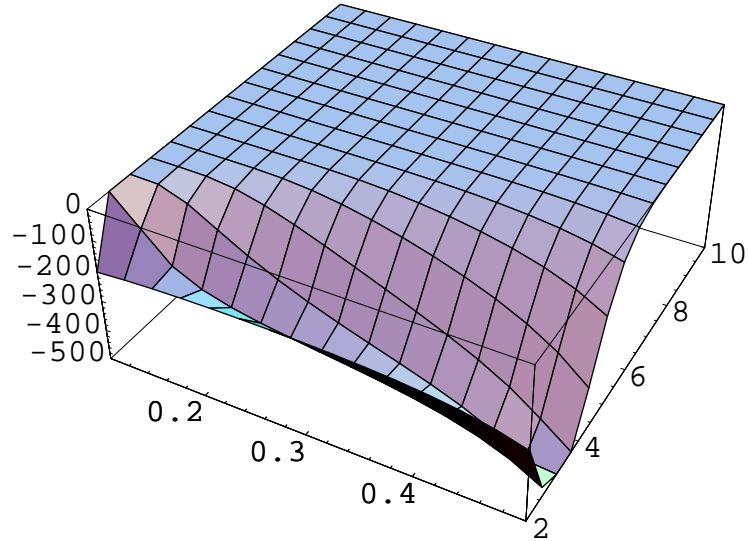


Fig. 15. Behaviour of  $\tilde{p}^3 W_6(\tilde{p}, y) F(\tilde{p}, y)$  (parabolic suppression 2).  $\Lambda = 10$ ,  $l = 0.5$ ,  $1.001/\Lambda \leq y \leq 0.99999l$ ,  $1/l \leq \tilde{p} \leq \Lambda$ . The contour of this graph is given later in Fig. 20.

dependent (D) on it.

**point 3** Regular (R) or singular (S) at  $y = 0$ .

**point 4** Symmetric for  $l\tilde{p} \leftrightarrow y/l$ .

**point 5** Symmetric for  $\tilde{p} \leftrightarrow 1/y$ , (Reciprocal symmetry).

**point 6** The Casimir energy is finite.

**point 7** Value of  $\alpha$ .

**point 8** Under  $Z_2$ -parity:  $y \leftrightarrow -y$ ;  $W(\tilde{p}, y)$  is even (E), odd (O) or none (N).

type	$W_1$	$W_{1b}$	$W_2$	$W_3$	$W_4$	$W_5$	$W_6$	$W_7$
point 1								
$l \rightarrow 0$	$l\delta(y)$	/	/	/	/	/	/	/
$l \rightarrow \infty$	$l^{-1} \times$	$l^{-1} \times$	/	/	$l^{-2} \times$	$l^{-3/2} \times$	$l^{-3/2} \times$	$l^{-2} \times$
	$\delta(\tilde{p})$	$\delta(\tilde{p})$	/	/	$\delta(\tilde{p}/y)$	$\delta(\sqrt{\tilde{p}}/y)$	$\delta(\tilde{p}/\sqrt{y})$	$\delta(\tilde{p}^2)$
point 2	$D$	$D$	$I$	$I$	$D$	$D$	$D$	$D$
point 3	$R$	$R$	$R$	$R$	$S$	$S$	$S$	$R$
point 4	$Y$	/	$Y$	$Y$	/	$N$	$N$	/
point 5	/	/	/	/	$Y$	$N$	$N$	/
point 6	$Y$	$Y$	$Y$	$Y$	$Y$	$Y$	$Y$	$Y$
point 7	2.5	2.5	0.060	0.092	2.5	2.5	2.5	2.5
point 8	$E$	$E$	$O$	$E$	$E$	$E$	$O$	$E$

type	$W_8$	$W_{47}$	$W_{56}$	$W_{88}$	$W_9$
point 1					
$l \rightarrow 0$	/	/	/	/	/
$l \rightarrow \infty$	$l^{-1} \times$	$l^{-2} \times$	$l^{-3/2} \times$	$l^{-2} \times$	$l^{-1} \times$
	$\delta(\sqrt{\tilde{p}^2 + \frac{1}{y^2}})$	$\delta(\tilde{p}\sqrt{\tilde{p}^2 + \frac{1}{y^2}})$	$\delta(\sqrt{\tilde{p}/y}\sqrt{\tilde{p} + \frac{1}{y}})$	$\delta(\tilde{p}^2 + \frac{1}{y^2})$	$\delta(\tilde{p} + \frac{1}{y})$
point 2	$D$	$D$	$D$	$D$	$D$
point 3	$S$	$S$	$S$	$S$	$S$
point 4	/	$N$	/	/	/
point 5	$Y$	$N$	$Y$	$Y$	$Y$
point 6	$Y$	$Y$	$Y$	$Y$	$Y$
point 7	2.5	2.6	2.5	2.6	2.5
point 8	$E$	$E$	$N$	$E$	$N$

So far as the legitimate reason of the introduction of  $W(\tilde{p}, y)$  is not clear, we should regard this procedure as a *regularization* for defining higher-dimensional theories. We give a definition of  $W(\tilde{p}, y)$  and a legitimate explanation in the next section. It should be conducted, in principle, consistently with the bulk geometry and the gauge principle.

### §7. Definition of weight function and dominant path

In the previous section, the weight function  $W(\tilde{p}, y)$  is introduced as some trial functions for suppressing the UV and IR divergences. In this section, we define (or specify) the weight function  $W(\tilde{p}, y)$  properly and give a *legitimate reason* for the introduction of  $W$ .

First, the requirement for controlling the  $\Lambda^5$ -divergence in § 4 led us to introduce some “damping” function  $W(\tilde{p}, y)$ , as in Eq.(6.1). Casimir energy is obtained by integrating out  $W(\tilde{p}, y)F(\tilde{p}, y)$  over the entire(5D) space region. Among all configurations involving the integral, there exists a dominant configuration that contributes

to the integral most dominantly. The present claim is that the dominant configuration should be fixed by the 5D geometry, that is, the 5D flat space(-time) with the periodic boundary condition and  $Z_2$ -symmetry. In the integral Eq.(6-1), the *dominant path*  $\tilde{p} = \tilde{p}_W(y)$  is characterized by the differential equation obtained by the variation method:  $\tilde{p} \rightarrow \tilde{p} + \delta\tilde{p}$ ,  $y \rightarrow y + \delta y$  in the  $(\tilde{p}, y)$ -integral expression Eq.(6-1). \*) Here, we *require*, on the basis of the present claim, that the dominant path  $\tilde{p}_W(y)$  coincides with the curve  $r = r_g(y)$  (or its momentum counterpart  $\tilde{p}_g(y)$ , (B-4)) which is determined by the minimal area condition Eq.(5-6). Note that the minimal area curve  $r = r_g(y)$  is defined by the 5D geometry. \*\*)

To explain the previous paragraph using only the coordinate  $(r = \sqrt{x^a x^a}, y)$ , we move to the coordinate expression by partial Fourier transformation. Casimir energy in Eq.(6-1) is re-expressed as

$$\begin{aligned} \hat{F}(r(x), y) &= \int \frac{d^4 p}{(2\pi)^4} e^{ipx} F(\tilde{p}, y) \quad , \quad \hat{W}(r(x), y) = \int \frac{d^4 p}{(2\pi)^4} e^{ipx} W(\tilde{p}, y) \quad , \\ r(x) &\equiv \sqrt{(x^1)^2 + (x^2)^2 + (x^3)^2 + (x^4)^2} \quad , \\ E_{Cas}^W(l) &= \int d^4 x \int_0^l dy \hat{W}(r(x), y) \hat{F}(r(x), y) = \\ &2\pi^2 \int_0^l dy \int_0^\infty dr \exp\{3 \ln r + \ln \hat{W}(r, y) + \ln \hat{F}(r, y)\} \quad . \quad (7-1) \end{aligned}$$

The unweighted case is  $\hat{W}(r(x), y) = \delta^4(x)$ ,  $W(\tilde{p}, y) = 1$ . The dominant contribution (path)  $r = r_W(y)$  to  $E_{Cas}^W$  is given by the *minimal 'action' principle*, that is, by applying the steepest-descend method to Eq.(7-1).

$$\frac{dr}{dy} = \frac{-\frac{1}{\hat{W}} \frac{\partial \hat{W}}{\partial y} - \frac{1}{\hat{F}} \frac{\partial \hat{F}}{\partial y}}{\frac{3}{r} + \frac{1}{\hat{W}} \frac{\partial \hat{W}}{\partial r} + \frac{1}{\hat{F}} \frac{\partial \hat{F}}{\partial r}} \equiv \hat{\mathcal{V}}_1(\hat{W}, \partial_r \hat{W}, \partial_y \hat{W}; r, y) \quad . \quad (7-2)$$

(The valley-bottom lines that appeared in Figs. 12–15 are regarded as the dominant paths.) Using the above result, we can obtain  $d^2 r / dy^2$ .

$$\begin{aligned} \hat{\mathcal{W}}_y &\equiv \frac{1}{\hat{W}} \frac{\partial \hat{W}}{\partial y} + \frac{1}{\hat{F}} \frac{\partial \hat{F}}{\partial y} \quad , \quad \hat{\mathcal{W}}_r \equiv \frac{1}{\hat{W}} \frac{\partial \hat{W}}{\partial r} + \frac{1}{\hat{F}} \frac{\partial \hat{F}}{\partial r} \quad , \\ \frac{d^2 r}{dy^2} &= -\frac{\partial_y \hat{\mathcal{W}}_y}{3r^{-1} + \hat{\mathcal{W}}_r} + \frac{\hat{\mathcal{W}}_y (\partial_r \hat{\mathcal{W}}_y + \partial_y \hat{\mathcal{W}}_r)}{(3r^{-1} + \hat{\mathcal{W}}_r)^2} - \frac{\hat{\mathcal{W}}_y^2 (-3r^{-2} + \partial_r \hat{\mathcal{W}}_r)}{(3r^{-1} + \hat{\mathcal{W}}_r)^3} \\ &\equiv \hat{\mathcal{V}}_2(\hat{W}, \partial_r \hat{W}, \partial_y \hat{W}, \partial_r^2 \hat{W}, \partial_y \partial_r \hat{W}, \partial_y^2 \hat{W}; r, y) \quad . \quad (7-3) \end{aligned}$$

\*) When  $W(\tilde{p}, y) = 1$ , the dominant path appears as  $\tilde{p}(y) \approx 0.75\Lambda$  (ind. of  $y$ ) in Figs. 2–4. This path, however, is “artificially” created by the UV cutoff. It is irrelevant to the 5D geometry. The differential equation of  $\tilde{p}_W(y)$  is obtained in Eq.(B-6).

\*\*) In § 5, we required the minimal area condition on the UV and IR regularization surfaces (boundary configuration), whereas, in this section, we require it on the dominant configuration in the  $(\tilde{p}, y)$  or  $(r, y)$ -integral appeared in the expression of Eq.(6-1). In other words, we have *fixed* the ‘dominant’ configuration (path), around which a small (“quantum”) fluctuation may occur, by taking the minimal surface curve.

We *require* here that the path  $r = r_W(y)$  of (7·2), which is defined in a  $\hat{W}(r, y)$ -dependent way, coincides with the minimal surface curve  $r_g(y)$  (5·6), which is defined independently of  $\hat{W}(r, y)$ . Hence,  $\hat{W}(r, y)$  is defined by inserting Eqs.(7·2) and (7·3) in Eq.(5·6):

$$\begin{aligned} & \hat{\mathcal{V}}_2(\hat{W}, \partial_r \hat{W}, \partial_y \hat{W}, \partial_r^2 \hat{W}, \partial_y \partial_r \hat{W}, \partial_y^2 \hat{W}; r, y) \\ & - \frac{3}{r} \{ \hat{\mathcal{V}}_1(\hat{W}, \partial_r \hat{W}, \partial_y \hat{W}; r, y) \}^2 - \frac{3}{r} = 0 \quad . \end{aligned} \quad (7·4)$$

We call this equation the ‘‘W-defining equation’’. It defines the weight function  $\hat{W}(r, y)$  in terms of the bulk metric (geometry) and model information  $\hat{F}$ . (Note:  $\hat{F}$  is given by Eq.(4·2).) In Appendix B.2, we treat the W-defining equation in  $(\tilde{p} = \sqrt{p^a p^a}, y)$  variables. Besides, how much the trial weight functions satisfy the above definition is numerically examined.

The scaling of the renormalized coupling  $g(y)$  is given by

$$\beta = -\frac{1}{4} \frac{1}{\frac{\partial}{\partial y} \ln r(y)} \frac{1}{g} \frac{\partial g}{\partial y} \quad , \quad (7·5)$$

where  $g(y)$  is a renormalized coupling at  $y$ . In the above derivation, Eq.(5·12) is used in the case  $\frac{\partial}{\partial y} r_{IR}(y) = 0$ , and  $r_{UV}(y) = r(y)$ .

## §8. Discussion and conclusion

Let us suppose that we have found the right weight function and that the divergences are successfully suppressed logarithmically. Casimir energy (2·24) is replaced by

$$8\pi^2 E_{Cas} = -\frac{3}{4} \frac{\zeta(5)}{l^4} (1 - 4c \ln(l\Lambda)) = -\frac{3}{4} \frac{\zeta(5)}{l'^4} \quad , \quad (8·1)$$

where  $c$  is some constant (see Eq.(6·5)). This shows that the periodicity parameter (or the compactification size)  $l$  changes as the renormalization scale changes. *The parameter  $l$  suffers from the renormalization effect.* It shows the field’s *interaction with the boundaries*. The above relation is *exact* because the present system is the *free* theory, and the heat-kernel (1-loop) approach can be regarded as a *complete (nonperturbative)* quantum treatment.<sup>21)</sup> Note that, in familiar 4D renormalizable interacting theories, the 1-loop effect is proportional to (coupling)<sup>2</sup>. In the present case, however,  $c$  is a *pure number*. When  $c$  is regarded small, i.e.,  $c \ll 1$ , we can approximate  $l'$  as <sup>\*)</sup>

$$l' \approx l(1 + c \ln(l\Lambda)) \quad , \quad (8·2)$$

The scaling behaviour of  $l$  is given by

$$\beta_l \text{ (\beta-function)} = \frac{\partial}{\partial(\ln \Lambda)} \ln \frac{l'}{l} = c \quad . \quad (8·3)$$

---

<sup>\*)</sup> From the results of Eq.(6·4),  $c \sim O(10^{-3})$ .

When  $c > 0$ , the compactification size  $l$  *grows (shrinks)* as the cutoff scale  $\Lambda$  *increases (decreases)*, whereas when  $c < 0$ ,  $l$  *shrinks (grows)* as the cutoff scale  $\Lambda$  *increases (decreases)*. The former case is expected. When  $c = 0$ , it means that the size  $l$  has no quantum effect. \*)

The present 5D geometry is flat. The interesting application is the warped case. The analysis is under way. Partial interesting results are obtained.<sup>26)–28)</sup> More or less, the arguments go similarly to that in the flat case except that the periodic and hyperbolic functions are replaced by the Bessel and modified Bessel ones. The essential difference is that one additional massive parameter, the 5D AdS curvature, appears in the expressions.  $E_{Cas}$  is expressed by the massive parameter in addition to  $l$  and  $\Lambda$ .

In the present standpoint, the space-time geometric field  $G_{MN}$  is regarded as a background one. It is *not* quantized. As for other bulk fields, we assume that they are renormalizable in the 3-brane. The role of the geometry appears when it is *required* that the dominant ‘path’, determined by the (EM) field quantization, coincides with the geometrically determined ‘path’ (*minimal area principle*). Practically  $W$  plays the role of suppressing the integral by weighting the original integrand. Although we have already stated the definition of  $W$  in § 7 and Appendix B, it is important to know the true meaning of  $W$ . In the next paragraph, we argue one possible interpretation.

In order to most naturally accomplish the above requirement, we can go to a new step. That is, we *propose* to *replace* the 5D space integral in Eq.(7.1) with the following *path integral*. Namely, we *newly define* Casimir energy in the higher-dimensional theory as follows:

$$\begin{aligned} \mathcal{E}_{Cas}(l, \Lambda) &\equiv \\ &\int_{1/\Lambda}^l d\rho \int_{\tilde{p}(0)=\tilde{p}(l)=1/\rho} \prod_{a,y} \mathcal{D}p^a(y) F(\tilde{p}, y) \exp \left[ -\frac{1}{2\alpha'} \int_0^l \frac{1}{\tilde{p}^3} \sqrt{\frac{\tilde{p}'^2}{\tilde{p}^4} + 1} dy \right] \\ &= \int_{1/\Lambda}^l d\rho \int_{r(0)=r(l)=\rho} \prod_{a,y} \mathcal{D}x^a(y) F\left(\frac{1}{r}, y\right) \exp \left[ -\frac{1}{2\alpha'} \int_0^l \sqrt{r'^2 + 1} r^3 dy \right] \quad , (8.4) \end{aligned}$$

where the limit  $\Lambda l \rightarrow \infty$  is taken and the surface (string) tension parameter  $1/2\alpha'$  is introduced (note: the dimension of  $\alpha'$  is  $[\text{length}]^4$ ).  $F(\tilde{p}, y)$  or  $F(1/r, y)$  is the energy density operator induced from the quantization of 5D EM fields in Eq.(3.22). The weight factor comes from the *area* suppression:

$\exp(-\text{Area}/2\alpha') = \exp[-(1/2\alpha') \int \sqrt{\det g_{ab}} d^4x]$ . In the above expression, we have followed the path-integral formulation of the density matrix (see Feynman’s text<sup>29)</sup>). The above definition clearly shows that the 4D space coordinates  $x^a$  or the 4D momentum coordinates  $p^a$  are *statistically quantized* with the Euclidean time  $y$  and the “*area Hamiltonian*”  $H = \int \sqrt{\det g_{ab}} d^4x$ . \*\*) This reminds us of the *space-time*

\*) In the unified theories based on the string theory,  $l$  is called the *moduli parameter* and is given by the vacuum expectation value of the dilaton field. How to fix the parameter is the moduli stabilization problem.

\*\*) The possibility of the quantum feature of the 5D coordinate/momenta was pointed out in

*uncertainty principle*<sup>30)</sup> introduced in the development of the string theory. The 5D quantum field theory leads to some *quantum statistical* system of the 4D coordinates  $\{x^a(y)\}$  with the inverse temperature parameter  $y$ . In this view, the treatment of § 6 and 7 is an *effective* action approach. We expect the direct evaluation of Eq.(8-4), numerically or analytically, leads to a similar result.

In the convincing regularization procedure, there should be some limiting process. In the explanation of the proposed one, before the previous paragraph, we do not clearly state the limiting process. We take large, but finite, values of  $\Lambda$  and  $l$  and obtain some formulae through numerical calculation valid for general (large but finite)  $\Lambda$  and  $l$ . \*) The limiting process should be given by

$$l\Lambda \rightarrow \infty \quad , \quad (8-5)$$

as in the proposed Eq.(8-4). In fact this limit is taken in the evaluation of the normalization constants of the weight functions in Eq.(6-1). When the limiting process Eq.(8-5) is taken into account, the physical quantity, that is, Casimir energy  $E_{Cas}$  (Eq.(8-1)) has the log divergence  $\ln(l\Lambda)$ . This divergence is subtracted by the renormalization procedure (8-1) and (8-2). (Note that the system is a locally free theory. It does not have the mass and coupling parameters. The original divergences must be absorbed away by the renormalization of the wave function or boundary parameter(s).) The anomalous scaling behavior Eq.(8-3) shows the non trivial interaction between the (free) fields and the boundaries.

In the present analysis, from the beginning, the extra space is treated differently from the 4D real space(-time). It is regarded as the part that provides the axis for a *scale* change. The change of renormalization group is determined by the *minimal area condition*. In order to extend the quantum field theory, without the divergence problem, the extra space should play a role in *suppressing* the singular behaviour. Although the geometry is treated as a background, the final outcome looks to demand some type of quantization among the 4D coordinates (or momenta) as explained in a previous paragraph. The necessity of the weight function  $W(\tilde{p}, y)$  in Eq.(6-1) can be interpreted to mean that we must take the well-defined space(-time) measure  $d^4p dy W(\tilde{p}, y)$ , instead of  $d^4p dy$  (Eq.(3-22) or (4-2)), in summing over 5D space(-time).

We have focused only on the vacuum energy. We must, of course, examine other physical quantities such as S-matrix amplitude in the interacting theories.

The present proposal should be compared with the string theory. We do not directly treat the string propagation. We start with quantizing the higher dimensional field theory in the standard way of QFT. We *require* the dominant configuration, the path  $r = r_W(y)$ , to be equal to the solution of the minimal area line  $r_g(y)$  by introducing the weight function  $W(\tilde{p}, y)$ . The bulk geometry takes part in the “coordinates quantization” by *fixing the central configuration* in this way. The closed-string-like configuration comes into this formalism through the *minimal area*

---

Ref.<sup>24)</sup> where the idea of the phase space  $(y, \tilde{p})$  was presented in relation to the divergence problem of the “deformed” propagator in the 5D bulk-boundary theory.

\*) This situation is similar to that in the *lattice gauge theory*.

*principle.* The field theories, which are applicable to this formalism, are limited to those that are renormalizable on the 3-brane, such as the 5D  $\Phi^4$ -theory, 5D YM theory, and 5D QED. However the advantages of this approach is that it is based on the QFT, hence we can expect various phenomenology applications. We stress the practical importance of calculation.

We have pointed out a possibility of quantizing higher dimensional field theories within QFT.

### Acknowledgements

Parts of this work have already been presented in the workshop “Evolution of Space-Time-Matter in the Early Universe” (07.5.29, Univ. of Tokyo, Japan), ICGA8 (07.8.29-9.1, Nara Women’s Univ., Japan), 62nd Japan Physical Society Meeting (07.9.21-24, Hokkaido Univ., Sapporo, Japan), KIAS-YITP Joint Workshop “Strings, Cosmology and Phenomenology” (07.9.24-28, Kyoto Univ., Japan), the workshop “Higher Dimensional Gauge Theory and the Unification of Forces” (07.11.29-30, Kobe Univ., Japan) and the workshop “Progress of String Theory and Quantum Field Theory” (07.12.7-10, Osaka City Univ.). The author thanks T. Inagaki (Hiroshima Univ.), K. Ito (TIT), T. Kawano (Univ. of Tokyo), M. Peskin (SLAC) and T. Yoneya (Univ. of Tokyo) for helpful comments and discussions on different occasions. He also thanks T. Tamaribuchi (Shizuoka Univ.) for advice in the computer calculation.

### Appendix A

#### — Minimal surface curve in 5D flat space —

We analytically examine the minimal area equation (5.6) in the 5D flat geometry.

$$3 - \frac{r\ddot{r}}{1 + \dot{r}^2} = 0 \quad , \quad 0 \leq y \leq l \quad , \quad (\text{A}\cdot 1)$$

where  $\dot{r} = dr/dy$  and  $\ddot{r} = d^2r/dy^2$ .

#### A.1. Classification of minimal surface curves

Before solving the equation, we classify all solutions using the differential equation above. This is useful in drawing minimal surface curves and confirming the noncrossing of curves. (The requirement comes from the renormalization-group flow interpretation of the curves. See a few sentences before Eq.(5.5).)

In terms of  $u \equiv 1/r^2$ , the above one (Eq.(A.1)) can be expressed as

$$u(y) \equiv \frac{1}{r(y)^2} = \frac{1}{x^a x^a} > 0 \quad ; \quad \ddot{u} = -6u^2 \leq 0 \quad , \quad 0 \leq y \leq l \quad . \quad (\text{A}\cdot 2)$$

From this equation, we can derive an important *inequality relation*:

$$\dot{u}|_{y=l} - \dot{u}|_{y=0} = -6 \int_0^l u^2 dy < 0 \quad . \quad (\text{A}\cdot 3)$$



The inequality  $\ddot{u} \leq 0$  in Eq.(A.2) implies that  $u(y)$  is convex upwards.

Making use of the above relation, we can classify all solutions (paths) as follows.

(i)  $\dot{u}(y=0) > 0$

(ia)  $\dot{u}(l) > 0$

In this case  $\dot{u}(y) > 0$  for  $0 \leq y \leq l$ .  $u(y)$  is simply increasing ( $r(y)$  is simply decreasing),

Fig.16

(ib)  $\dot{u}(l) < 0$

(ib $\alpha$ )  $u(0) < u(l)$  Fig. 17

(ib $\beta$ )  $u(0) > u(l)$  Fig. 18

(ii)  $\dot{u}(y=0) < 0$

$u(y)$  is simply decreasing ( $r(y)$  is simply increasing), Fig. 19

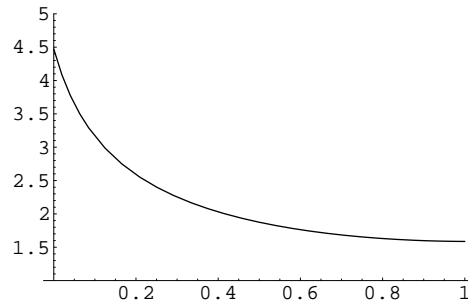


Fig. 16. Geodesic curve  $r(y)$  of Eq.(A.1) by Runge-Kutta method. Type (ia) simply decreasing.  $r(0) = 4.472$ ,  $\dot{r}(0) = -22.36$

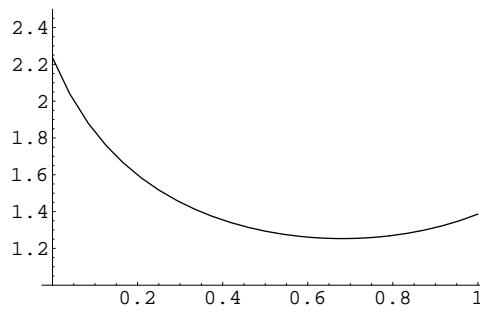


Fig. 17. Geodesic curve  $r(y)$  of Eq.(A.1) by Runge-Kutta method. Type (ib $\alpha$ ).  $r(0) = 2.236$ ,  $\dot{r}(0) = -5.590$ .

Although numerical solutions are displayed in Figs. 16–19, the general analytic solution is given in Appendix A.2. We have confirmed the high-precision equality between the numerical curves and the analytical ones.

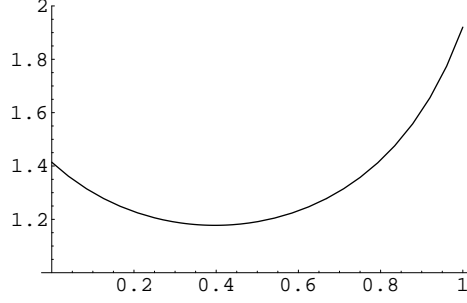


Fig. 18. Geodesic curve  $r(y)$  of Eq.(A.1) by Runge-Kutta method. Type (ib $\beta$ ).  $r(0) = 1.4142$ ,  $\dot{r}(0) = -1.4142$ .

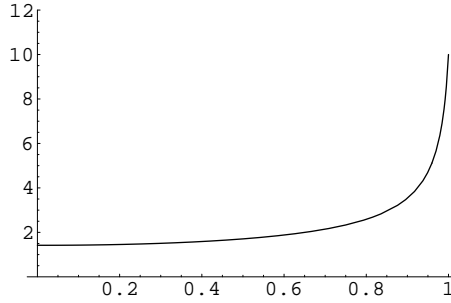


Fig. 19. Geodesic curve  $r(y)$  of Eq.(A.1) by Runge-Kutta method. Type (ii) simply increasing.  $r(1.0) = 10.0$ ,  $\dot{r}(1.0) = 350.0$ .

#### A.2. General analytic solution of minimal surface curve (Eq.(5.6), (A.1), or (A.2))

We solve the differential equation (Eq(refsurf2), (A.1), or (A.2)), which is the minimal surface trajectory of the 5D *flat* geometry. The first integral is given by

$$\begin{aligned} \frac{d}{dy} \left( \frac{1}{2} \dot{u}^2 + 2u^3 \right) &= 0 \quad , \\ \frac{1}{2} \dot{u}^2 + 2u^3 &= 2C \quad , \quad C (> 0) : \text{an integral constant} \\ \dot{u} = \frac{du}{dy} &= \pm 2\sqrt{C - u^3} \quad , \quad 0 < u \leq \sqrt[3]{C} \quad . \end{aligned} \quad (\text{A.4})$$

We see that the present classical system is equivalent to one particle mechanics with the potential  $V = 2u^3$ . The second integral is obtained as follows:

$$\int \frac{du}{\sqrt{C - u^3}} = \pm 2 \int dy = \pm 2y + C' \quad , \quad C' : \text{another integral constant} \quad , \quad (\text{A.5})$$

The LHS of the above equation can be integrated as

$$\begin{aligned} v &\equiv \frac{u}{\sqrt[3]{C}} \quad , \quad 0 < v \leq 1 \quad , \\ \int \frac{du}{\sqrt{C - u^3}} &= \frac{\sqrt[3]{C}}{\sqrt{C}} \int \frac{dv}{\sqrt{1 - v^3}} = -\frac{C^{-1/6}}{\sqrt[4]{3}} F \left( \cos^{-1} \frac{\sqrt{3} - 1 + v}{\sqrt{3} + 1 - v}, \frac{\sqrt{3} + 1}{2\sqrt{2}} \right) \quad (\text{A.6}) \end{aligned}$$

where  $F(\varphi, k)$  is the *elliptic integral of the first kind* and the following integral formula is used.

$$\int_v^1 \frac{dx}{\sqrt{1-x^3}} = \frac{1}{\sqrt[4]{3}} F\left(\cos^{-1} \frac{\sqrt{3}-1+v}{\sqrt{3}+1-v}, \frac{\sqrt{3}+1}{2\sqrt{2}}\right), \quad 0 < \frac{\sqrt{3}-1+v}{\sqrt{3}+1-v} \leq 1, \quad ,$$

$$F(\varphi, k) = \int_0^\varphi \frac{d\theta}{\sqrt{1-k^2 \sin^2 \theta}} = \int_0^{z_1} \frac{dz}{\sqrt{(1-z^2)(1-k^2 z^2)}} \equiv \tilde{F}(z_1, k), \quad ,$$

$$0 \leq k \leq 1, \quad -\frac{\pi}{2} < \varphi < \frac{\pi}{2}, \quad z_1 \equiv \sin \varphi = \text{sn}(\tilde{F}, k) \text{(A;7)}$$

where  $\text{sn}(\tilde{F}, k)$  is defined by the inverse function of  $\tilde{F}(z_1, k)$  and is called *Jacobi's elliptic function*. It has the period  $4K(k) \equiv 4F(\frac{\pi}{2}, k)$ . Hence,

$$z_1 = \sin \varphi = \pm \sqrt{1 - \cos^2 \varphi} = \pm \{(1 - \cos \varphi)(1 + \cos \varphi)\}^{1/2}$$

$$= \pm \frac{2\sqrt[4]{3}\sqrt{1-v}}{\sqrt{3}+1-v} = \text{sn}\left(-\sqrt[4]{3}C^{1/6}(\pm 2y + C'), \frac{\sqrt{3}+1}{2\sqrt{2}}\right). \quad \text{(A.8)}$$

We can solve the above equation w.r.t.  $v = \frac{u}{\sqrt[3]{C}}$ . \*)

$$u_+ = \frac{1}{r_+^2} = \sqrt[3]{C} \frac{(\sqrt{3}+1)\bar{\text{sn}}_+^2 - 2\sqrt{3}(1-|\bar{\text{cn}}_+|)}{\bar{\text{sn}}_+^2}, \quad ,$$

$$u_- = \frac{1}{r_-^2} = \sqrt[3]{C} \frac{(\sqrt{3}+1)\bar{\text{sn}}_-^2 - 2\sqrt{3}(1-|\bar{\text{cn}}_-|)}{\bar{\text{sn}}_-^2}, \quad ,$$

$$\bar{\text{sn}}_\pm(y, C, C') \equiv \text{sn}\left(-\sqrt[4]{3}C^{1/6}(\pm 2y + C'), \frac{\sqrt{3}+1}{2\sqrt{2}}\right), \quad ,$$

$$\bar{\text{cn}}_\pm(y, C, C') \equiv \text{cn}\left(-\sqrt[4]{3}C^{1/6}(\pm 2y + C'), \frac{\sqrt{3}+1}{2\sqrt{2}}\right). \quad \text{(A.9)}$$

From the requirement  $u = \frac{1}{r^2} > 0$ , the above result indicates that \*\*)

$$\frac{\sqrt{3}-1}{\sqrt{3}+1} \leq |\bar{\text{cn}}_\pm(y, C, C')| = \left| \text{cn}\left(-\sqrt[4]{3}C^{1/6}(\pm 2y + C'), \frac{\sqrt{3}+1}{2\sqrt{2}}\right) \right| \leq 1. \quad \text{(A.10)}$$

We must choose  $C$  and  $C'$  in such a way that the above relation is valid for  $\forall y \in (0, l)$ .  $r(y=0)$  and  $\left.\frac{dr}{dy}\right|_{y=0}$  are related to  $C$  and  $C'$  as follows:

$$r(0) = C^{-1/6} \frac{|\text{sn}0(C, C')|}{\{(\sqrt{3}+1)\text{sn}0(C, C')^2 - 2\sqrt{3}(1-|\text{cn}0(C, C')|)\}^{1/2}}, \quad ,$$

\*) Note that one of two solutions (of a quadratic equation w.r.t.  $v$ ) is omitted here because of  $(\sqrt{3}+1)\bar{\text{sn}}^2 - 2\sqrt{3}(1-|\bar{\text{cn}}|) = -\{(\sqrt{3}+1)|\bar{\text{cn}}| + \sqrt{3}-1\}\{|\bar{\text{cn}}|+1\} < 0$ .

\*\*) Using the relation  $\bar{\text{sn}}^2 = 1 - \bar{\text{cn}}^2$ , we know that  $(\sqrt{3}+1)\bar{\text{sn}}^2 - 2\sqrt{3}(1-|\bar{\text{cn}}|) = \{\sqrt{3}-1 - (\sqrt{3}+1)|\bar{\text{cn}}|\}\{|\bar{\text{cn}}|-1\}$ .

$$\begin{aligned}
\operatorname{sn}0(C, C') &= \operatorname{sn} \left( -\sqrt[4]{3} C^{1/6} C', \frac{\sqrt{3}+1}{2\sqrt{2}} \right) , \\
\operatorname{cn}0(C, C') &= \operatorname{cn} \left( -\sqrt[4]{3} C^{1/6} C', \frac{\sqrt{3}+1}{2\sqrt{2}} \right) , \\
\left. \frac{dr}{dy} \right|_{y=0} &= \mp r(0)^3 \sqrt{C - \frac{1}{r(0)^6}} , \\
r_+(l) &= C^{-1/6} \frac{|\bar{\operatorname{sn}}_+(l, C, C')|}{\{(\sqrt{3}+1)\bar{\operatorname{sn}}_+(l, C, C')^2 - 2\sqrt{3}(1 - |\bar{\operatorname{cn}}_+(l, C, C')|)\}^{1/2}} , \\
r_-(l) &= C^{-1/6} \frac{|\bar{\operatorname{sn}}_-(l, C, C')|}{\{(\sqrt{3}+1)\bar{\operatorname{sn}}_-(l, C, C')^2 - 2\sqrt{3}(1 - |\bar{\operatorname{cn}}_-(l, C, C')|)\}^{1/2}} . \quad (\text{A}\cdot 11)
\end{aligned}$$

The two integration constants come from the second-derivative differential equation (A·1). In the numerical approach of the Runge-Kutta method, the constants are given by  $r(y=0)$  and  $\left. \frac{dr}{dy} \right|_{y=0}$ . It is important to check, in the simple case of the flat model, that the numerical solution correctly produces the analytic one. In the warped case, we rely only on the numerical method.

## Appendix B

### — Weight function and minimal surface curve —

In § 7, we have presented a specification of the weight function  $W(\tilde{p}, y)$ . Here, we examine its validity by numerically evaluating the consistency equation, to be given later, for each  $W$  that appeared in Eq.(6·1).

#### B.1. Reciprocal space

The 4D boundary manifold described in § 5 is characterized by the metric,

$$\begin{aligned}
ds^2 &= \left( \delta_{ab} + \frac{x^a x^b}{(r \frac{dr}{dy})^2} \right) dx^a dx^b \equiv g_{ab}(x) dx^a dx^b , \quad r = \sqrt{x^a x^a} , \\
(\delta_{ab}) &= \operatorname{diag}(1, 1, 1, 1), \quad A = \int \sqrt{\det g_{ab}} d^4x = \int_{1/\Lambda}^l \sqrt{r'^2 + 1} r^3 dy, \quad r' = \frac{dr}{dy}, \quad (\text{B}\cdot 1)
\end{aligned}$$

where  $\{x^a; a = 1, 2, 3, 4\}$  are the coordinates of the 4D Euclidean space manifold. We introduce the reciprocal coordinates  $\{p^a\}$  defined by

$$x^a = \frac{p^a}{p^2} , \quad p^2 \equiv p^a p^a ; \quad p^a = \frac{x^a}{x^2} , \quad x^2 \equiv x^a x^a ; \quad x^2 = \frac{1}{p^2} . \quad (\text{B}\cdot 2)$$

The metric (B·1) can be, in terms of these coordinates, rewritten as

$$\begin{aligned}
dx^a &= \frac{1}{p^2} (-\delta^{ab} + 2Q^{ab}) dp^b , \quad Q^{ab} \equiv \delta^{ab} - \frac{p^a p^b}{p^2} , \\
Q^{ab} &= Q^{ba} , \quad p^a Q^{ab} = 0 , \quad Q^{ab} p^b = 0 , \quad Q^{ab} Q^{bc} = Q^{ac} , \quad \delta^{ab} Q^{ab} = 3 ,
\end{aligned}$$

$$ds^2 = \frac{1}{(p^2)^2} \left( \delta_{ab} + p^2 \frac{p^a p^b}{\left(\frac{dp}{dy}\right)^2} \right) dp^a dp^b \equiv \hat{g}_{ab}(p) dp^a dp^b \quad , \quad \tilde{p} = \sqrt{p^a p^a} \quad . \quad (\text{B}\cdot 3)$$

The 4D volume (the area of the boundary surface) is given by

$$\begin{aligned} A &= \int \sqrt{\det \hat{g}_{ab}} d^4 p = \int \sqrt{1 + \frac{\tilde{p}^4}{\left(\frac{d\tilde{p}}{dy}\right)^2}} \frac{d\tilde{p}}{\tilde{p}^5} \\ &= \int_{1/\Lambda}^l \sqrt{\left(\frac{\tilde{p}'}{\tilde{p}^2}\right)^2 + 1} \tilde{p}^{-3} dy \quad , \quad \tilde{p}' \equiv \frac{d\tilde{p}}{dy} \quad , \end{aligned} \quad (\text{B}\cdot 4)$$

where the  $S^3$  property:  $\tilde{p} = 1/\sqrt{x^2} = r(y)^{-1} = \tilde{p}(y)$  is used.  $\Lambda$  is the UV cutoff for the 4D momentum integral. The minimal area principle gives the equation,

$$\begin{aligned} \tilde{p}(y) &\rightarrow \tilde{p}(y) + \delta\tilde{p}(y) \quad , \quad \delta\mathcal{A} = 0 \quad , \\ 3 + \frac{(\tilde{p}''\tilde{p} - 2\tilde{p}'^2)/\tilde{p}^4}{1 + (\tilde{p}'/\tilde{p}^2)^2} &= 0 \quad \text{or} \quad \frac{d^2\tilde{p}}{dy^2} + \frac{1}{\tilde{p}} \left(\frac{d\tilde{p}}{dy}\right)^2 + 3\tilde{p}^3 = 0 \quad . \end{aligned} \quad (\text{B}\cdot 5)$$

This equation is the same as Eq.(5-6) expressed by  $r(=1/\tilde{p})$ .

## B.2. Numerical confirmation of the relation between weight function and minimal surface curve

The dominant configuration (path,  $\tilde{p} = \tilde{p}(y)$ ) for Casimir energy Eq.(6-1) is given by an ordinary variation method (minimal ‘‘action’’ principle).

$$\begin{aligned} y &\rightarrow y + \delta y \quad , \\ \delta\{W(\tilde{p}(y), y)\tilde{p}^3(y)F(\tilde{p}(y), y)\} &= \delta y \left( \frac{d\tilde{p}}{dy} \frac{\partial}{\partial\tilde{p}} + \frac{\partial}{\partial y} \right) (\tilde{p}^3 W(\tilde{p}, y) F(\tilde{p}, y)) = 0, \\ \frac{d\tilde{p}}{dy} &= \frac{-\frac{\partial \ln(WF)}{\partial y}}{\frac{3}{\tilde{p}} + \frac{\partial \ln(WF)}{\partial\tilde{p}}} \quad , \end{aligned} \quad (\text{B}\cdot 6)$$

where  $W(\tilde{p}, y)$  is the weight function ‘practically’ introduced in § 6 and is properly defined in § 7 using 5D coordinates  $(r, y)$ . In this subsection, we define  $W(\tilde{p}, y)$  using  $(\tilde{p}, y)$ .  $F(\tilde{p}, y)$  is given in Eq.(4-2). The coordinate version of the above result is given in the text (Eq.(7-2)). We can also obtain  $d^2\tilde{p}/dy^2$ .

$$\begin{aligned} \mathcal{W}_y &\equiv \partial_y \ln(WF) \quad , \quad \mathcal{W}_{\tilde{p}} \equiv \partial_{\tilde{p}} \ln(WF) \quad , \\ \frac{d\tilde{p}}{dy} &= -\frac{\mathcal{W}_y}{3\tilde{p}^{-1} + \mathcal{W}_{\tilde{p}}} \equiv \mathcal{V}_1(W, \partial_{\tilde{p}}W, \partial_y W; \tilde{p}, y) \quad , \\ \frac{d^2\tilde{p}}{dy^2} &= -\frac{\partial_y \mathcal{W}_y}{3\tilde{p}^{-1} + \mathcal{W}_{\tilde{p}}} + \frac{\mathcal{W}_y(\partial_{\tilde{p}}\mathcal{W}_y + \partial_y \mathcal{W}_{\tilde{p}})}{(3\tilde{p}^{-1} + \mathcal{W}_{\tilde{p}})^2} - \frac{\mathcal{W}_y^2(-3\tilde{p}^{-2} + \partial_{\tilde{p}}\mathcal{W}_{\tilde{p}})}{(3\tilde{p}^{-1} + \mathcal{W}_{\tilde{p}})^3} \\ &\equiv \mathcal{V}_2(W, \partial_{\tilde{p}}W, \partial_y W, \partial_{\tilde{p}}^2W, \partial_y \partial_{\tilde{p}}W, \partial_y^2W; \tilde{p}, y) \quad . \end{aligned} \quad (\text{B}\cdot 7)$$

Note that the RHSs of the expressions  $d\tilde{p}/dy$  and  $d^2\tilde{p}/dy^2$  above are functions of  $\tilde{p}$  and  $y$ . If we consider that  $W(\tilde{p}, y)$  is unknown, by inserting the above ones in

Eq.(B·5), we obtain a partial differential equation for  $W(\tilde{p}, y)$  involving up to 2nd derivative. We call it the “W-defining equation”.

$$\text{W-defining Equation : } \mathcal{V}_2 + \frac{1}{\tilde{p}}\mathcal{V}_1^2 + 3\tilde{p}^3 = 0 \quad , \quad (\text{B}\cdot 8)$$

where  $\mathcal{V}_1$  and  $\mathcal{V}_2$  are defined in Eq.(B·7). We consider that the 2nd-derivative differential equation defines the weight function  $W(\tilde{p}, y)$ . It is difficult to solve it. Here, we are content with a numerical consistency check.

If we take some example of  $W(\tilde{p}, y)$  appearing in Eq.(6·1), the dominant configuration  $\tilde{p}_W = \tilde{p}_W(y)$  is graphically shown by the valley-bottom line of Casimir energy integrand  $W(\tilde{p}, y)\tilde{p}^3 F(\tilde{p}, y)$ , (see Figs. 12–15). On the other hand, there exists another path  $\tilde{p}_g(y)$  that is the minimal surface curve of the bulk geometry, that is, Eq.(5·6) or (B·5).  $\tilde{p}_g(y)$  is determined by the 5D metric, and is completely independent of both the weight  $W$  and the model  $F$ . \*) The W-defining equation above represents the equality  $\tilde{p}_W(y) = \tilde{p}_g(y)$ . We can numerically compare  $\tilde{p}_W(y)$  and  $\tilde{p}_g(y)$ . We show, in Fig. 20, the contour of Fig. 15 (parabolic suppression

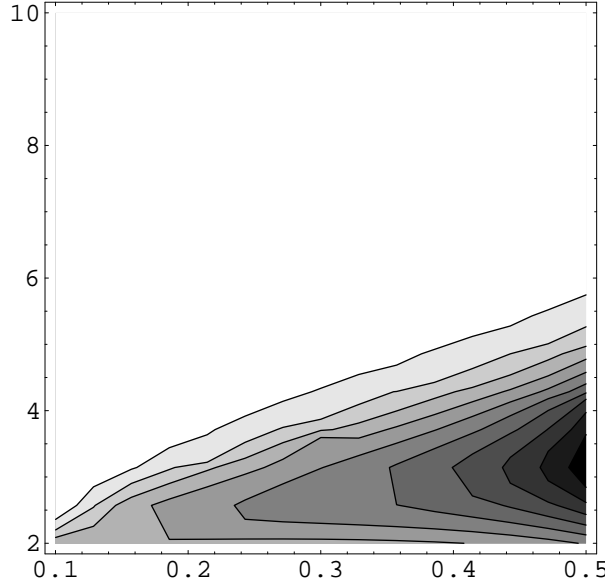


Fig. 20. Contour of  $\tilde{p}^3 W_6(\tilde{p}, y) F(\tilde{p}, y)$  (parabolic suppression 2, Fig. 15).  $\Lambda = 10$ ,  $l = 0.5$ . Horizontal axis:  $1.001/\Lambda \leq y \leq 0.99999l$ ; vertical axis:  $1/l \leq \tilde{p} \leq \Lambda$ .

W6). We can see the valley-bottom line as  $\tilde{p}_W(y) \approx 4.3\sqrt{y}$ . In Fig. 21, we show the minimal surface curve  $\tilde{p}_g(y) = 1/r_g(y)$ , which is the  $r_-(y)$  solution with  $C = 5.1215$  and  $C' = 1.068$  in Eq.(A·9) of Appendix A.2. The two graphs are similar, at least in shape and magnitude order. For other weights, we confirm a similar situation.

\*) Precisely, the boundary conditions at  $y = 0$  and  $y = l$  (boundary values:  $\tilde{p}(0)$  and  $\tilde{p}(l)$ ) are also necessary.

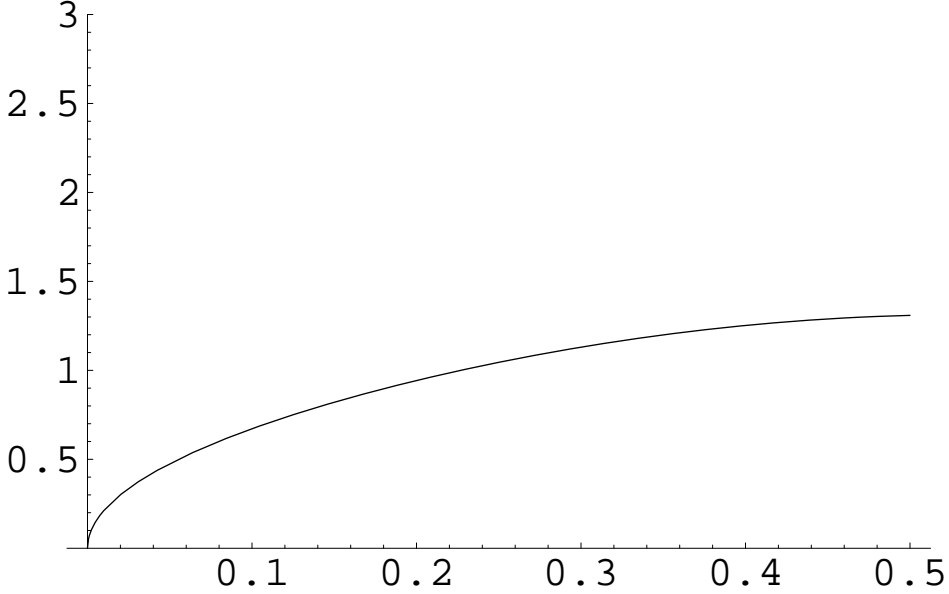


Fig. 21. Minimal surface curve  $1/r_-(y)$ ,  $C = 5.1215$ ,  $C' = 1.068$  in Eq.(A-9). Horizontal axis:  $0 \leq y \leq 0.5$ ; vertical axis:  $0 \leq 1/r_- \leq 3$ .

### Appendix C

— Numerical evaluation of scaling laws:  $E_{Cas}$  (4.5),  $E_{Cas}^{RS}$  (5.1), and  $E_{Cas}^W$  (6.4)

In the text, (regularized) Casimir energy is numerically calculated in three ways: 1) original version (rectangle-region integral), 2) restricted-region integral ( Randall-Sundrum type ), 3) weighted version. The final expressions show the *scaling* behaviors about the boundary (extra-space) parameter  $l$  and the 4D momentum cutoff  $\Lambda$ . The results are crucial for the present conclusion. Hence, we explain here how the numerical results are obtained.

First, let us take the unweighted case with the rectangle integral region (original form) of Casimir energy (4.2).

$$2^3 \pi^2 E_{Cas}(\Lambda, l) = \int_{1/l}^{\Lambda} d\tilde{p} \int_{1/\Lambda}^l dy \tilde{p}^3 F(\tilde{p}, y) \quad , \quad (C.1)$$

where  $\tilde{p}^3 F(\tilde{p}, y)$  is explicitly given in Eq.(4.4). The integral region is graphically shown in Fig. 1 as a rectangle ( $\epsilon = 1/\Lambda, \mu = 1/l$ ). The graphs of the integrand of (C.1),  $\tilde{p}^3 F(\tilde{p}, y)$ , are shown for  $(l, \Lambda) = (1, 10)$  [Fig. 2],  $(1, 100)$  [Fig. 3],  $(1, 1000)$  [Fig. 4], in the text. From the behaviors we can expect that  $E_{Cas}(\Lambda, l)$ , (C.1), leadingly behaves as  $\Lambda^5$ , because the depth of the valleys, shown in Figs. 2–4, is proportional to  $\Lambda^4$  and the graph-behaviors are monotonic along the y-axis (except near the boundaries  $y = 1/\Lambda$  and  $l$ ). It is confirmed by directly evaluating Eq.(C.1) numerically (the numerical integral in Ref.31). We plot the numerical results for various  $\Lambda$  and  $l$  values in Fig. 22. From the straight-line behavior we can safely fit the curve as

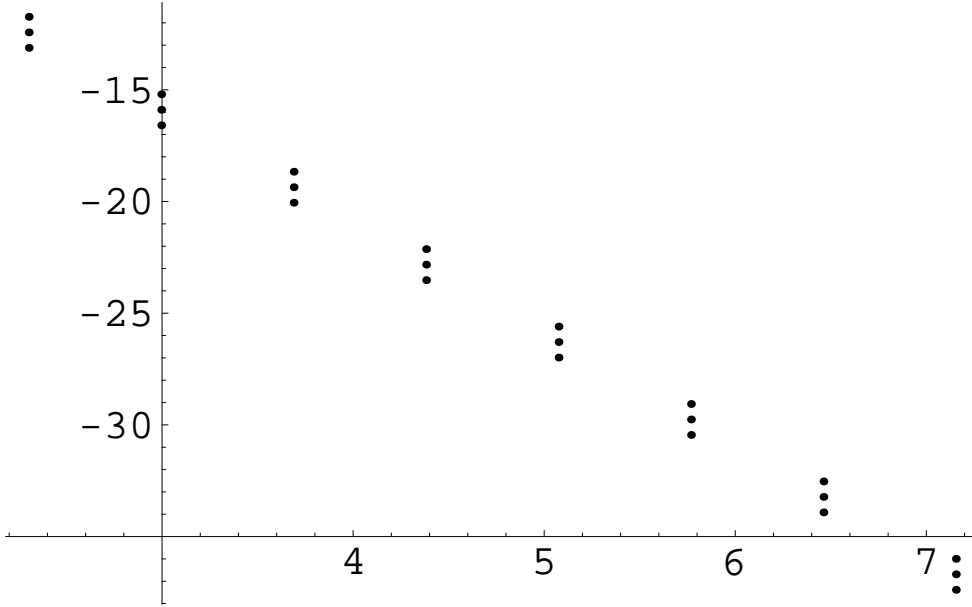


Fig. 22. Casimir Energy  $E_{Cas}$  of (C·1) for various  $(\Lambda, l)$  values. Horizontal axis:  $\ln \Lambda$  ( $\Lambda = 10, 20, 40, \dots, 1280$ ); vertical axis:  $-\ln(|2^3 \pi^2 E_{Cas}|)$ . The results are grouped into three lines. The values placed on the top, middle, and bottom lines correspond to  $l = 10, 20$ , and  $40$  respectively.

$2^3 \pi^2 E_{Cas} = l \Lambda^5 (a_5 + b_5 \ln(l\Lambda))$ . The best fit is given by (manipulating numerical data in Ref.31))

$$2^3 \pi^2 E_{Cas}(\Lambda, l) = -0.1249 l \Lambda^5 - (1.41, 0.706, 0.353) \times 10^{-5} l \Lambda^5 \ln(l\Lambda) \quad . \quad (C\cdot2)$$

The triplet results correspond to  $l = 10, 20$  and  $40$ . The first term is firmly fixed (the number of significant figures (NSF) is 4), whereas the second term is unstable (the coefficients are proportional to  $1/l$ ). The second one is numerically small compared with the first, and its determination requires more careful treatment of small numbers. To determine it firmly, calculation using larger values of  $\Lambda$  and  $l$  is necessary.

In the restricted region case, Eq.(5·1), we do the numerical integral of the following expression,

$$2^3 \pi^2 E_{Cas}^{RS} = \int_{1/l}^{\Lambda} dq \int_{1/\Lambda}^{1/q} dy q^3 F(q, y) = \int_{1/\Lambda}^l du \int_{1/l}^{1/u} d\tilde{p} \tilde{p}^3 F(\tilde{p}, u) \quad . \quad (C\cdot3)$$

We plot the results in Fig. 23 for various values of  $\Lambda$  and  $l$ . From the straight line behavior, we can safely fit the curve as  $2^3 \pi^2 E_{Cas}^{RS} = \Lambda^4 (a_4 + b_4 \ln(l\Lambda))$ . The best fit is given by

$$2^3 \pi^2 E_{Cas}^{RS}(\Lambda, l) = -8.93814 \times 10^{-2} \Lambda^4 + (+7.73, -4.83, +5.00) \times 10^{-10} \Lambda^4 \ln(l\Lambda) \quad . \quad (C\cdot4)$$



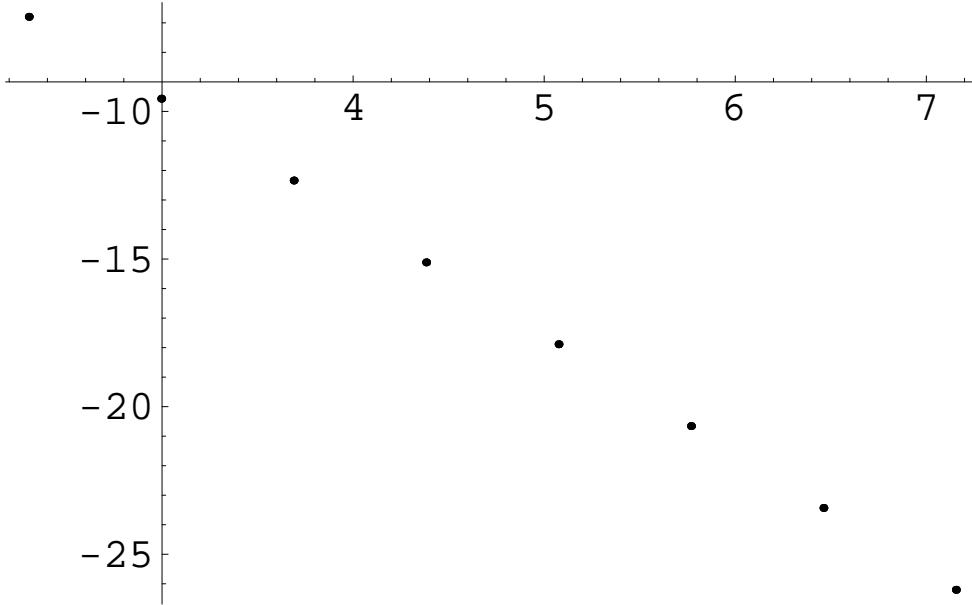


Fig. 23. Casimir Energy  $E_{Cas}^{RS}$  of (C-3) for various values  $(\Lambda, l)$ . Horizontal axis:  $\ln \Lambda$  ( $\Lambda = 10, 20, 40, \dots, 1280$ ); vertical axis:  $-\ln(|2^3 \pi^2 E_{Cas}^{RS}|)$ . The results are placed on a straight line for different  $\Lambda$  and overlap (within the presented dots) for three different values of  $l = 10, 20$ , and 40.

The triplet results corresponds to  $l = 10, 20$ , and 40. The first term is firmly fixed (the NSF is 6), whereas the second term is unstable. The second one is numerically very small compared with the first, and we may say that the second term vanishes within the present numerical precision.

Finally, we explain the weighted case in Eq.(6-1) taking the elliptic type  $W_1$  as an example.

$$2^3 \pi^2 E_{Cas}^{W_1}(\Lambda, l) = \int_{1/l}^{\Lambda} d\tilde{p} \int_{1/\Lambda}^l dy \tilde{p}^3 W_1(\tilde{p}, y) F(\tilde{p}, y) \quad ,$$

$$W_1(\tilde{p}, y) = \frac{1}{N_1} e^{-\frac{l^2}{2} \tilde{p}^2 - \frac{1}{2l^2} y^2} \quad , \quad N_1 = \frac{1.557}{8\pi^2} \quad , \quad (\text{C-5})$$

where the UV cutoff  $\Lambda$  and IR cutoff  $l$  are introduced to see the scaling behavior. In Fig. 24, we show the numerical results of  $E_{Cas}^{W_1}(\Lambda, l) \times N_1$  for different  $\Lambda$  and  $l$  values. (Note that the axes of Fig. 24 are on a linear scale, not on a log scale.) From the straight line behavior of Fig. 24, we can safely fit the curve as  $2^3 \pi^2 E_{Cas}^{W_1} \times N_1 = (A/l)(a_1 + b_1 \ln(l\Lambda))$ . The best fit is given by

$$2^3 \pi^2 E_{Cas}^{W_1}(\Lambda, l) \times N_1 = -(3.892, 3.894, 3.894) \frac{\Lambda}{l^3} + (-0.221, 1.70, 1.76) \times 10^{-4} \frac{\Lambda \ln(l\Lambda)}{l^3} \quad (\text{C-6})$$

The triplet results correspond to  $l = 10, 20$ , and 40. The first term is firmly fixed (the NSF is 3 at least), whereas the second term is unstable. This data shows that the coefficients become stable as  $l$  increase. As for other types of  $W$ , the best fit

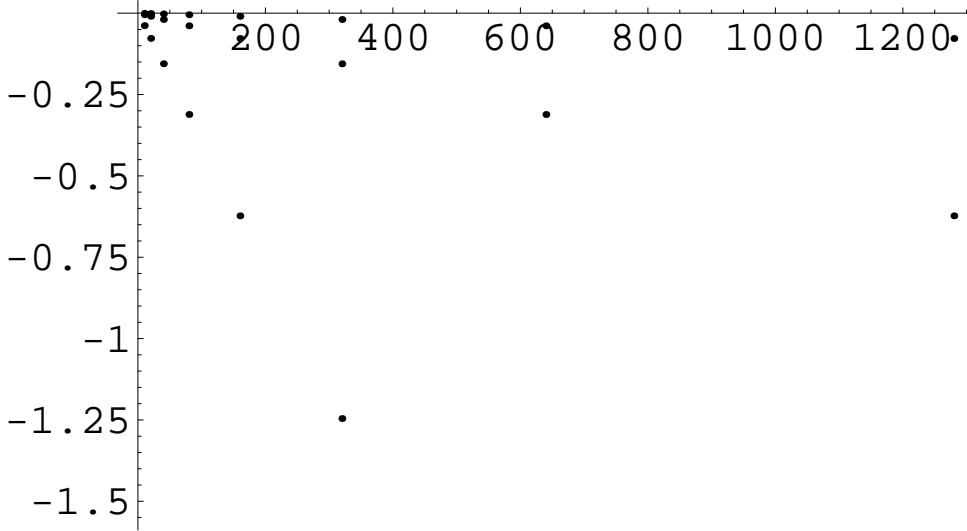


Fig. 24. Casimir Energy  $E_{Cas}^{W_1}$  of (C.5) for various  $(\Lambda, l)$  values. Horizontal axis:  $\Lambda$  ( $\Lambda = 10, 20, 40, \dots, 1280$ ); vertical axis:  $2^3 \pi^2 E_{Cas}^{W_1} \times N_1$ . The results are grouped into three lines. The values placed on the top, middle, and bottom lines correspond to  $l = 40, 20$ , and  $10$  respectively.

scaling behaviors are listed in Eq.(6.4) of the text. The behaviors taking  $W_2$  and  $W_3$  are different from the others. This is because the normalization factors  $N_2$  and  $N_3$  are divergent. The leading values, except  $W_2$  and  $W_3$ , do not so much depend on the choice of  $W$ .

### References

- 1) Th. Kaluza, Sitzungsberichte der K. Preussischen (Akademie der Wissenschaften, Berlin, 1921), p.966.
- 2) O. Klein, Z. Phys. **37** (1926),895.
- 3) T. Appelquist and A. Chodos, Phys. Rev. D **28** (1983), 772.  
T. Appelquist and A. Chodos, Phys. Rev. Lett. **50** (1983), 141.
- 4) M. Bordag, U. Mohideen and V. M. Mostepanenko, Phys. Rep. **353** (2001), 1 ,  
quant-ph/0106045.
- 5) N. Arkani-Hamed, A. G. Cohen and H. Georgi, Phys. Rev. Lett. **86** (2001), 4757 ,  
hep-th/0104005.
- 6) C. T. Hill, S. Pokorski and J. Wang, Phys. Rev. D **64** (2001), 105005 , hep-th/0104035.
- 7) F. Bauer, M. Lindner and G. Seidl, J. High Energy Phys. **05** (2004), 026 , hep-th/0309200.
- 8) L. Randall, M. D. Schwartz and S. Tambyahpillai, J. High Energy Phys. **10** (2005), 110  
, hep-th/0507102.
- 9) L. Randall and M. D. Schwartz, J. High Energy Phys. **11** (2001), 003 , hep-th/0108114.
- 10) S. Ichinose and A. Murayama, Phys. Rev. D **76** (2007), 065008 , hep-th/0703228.
- 11) D. Z. Freedman, S. D. Mathur, A. Matusis and L. Rastelli, Nucl. Phys. B **546** (1999), 96  
, hep-th/9804058.
- 12) M. Henningson and K. Skenderis, J. High Energy Phys. **07** (1998), 023 , hep-th/9806087.
- 13) J. Distler and F. Zamora, Adv. Theor. Math. Phys. **2** (1999), 1405, hep-th/9810206.
- 14) L. Girardello, M. Petrini, M. Porrati and A. Zaffaroni, J. High Energy Phys. **12** (1998),  
022 , hep-th/9810126.

- 15) M. Porrati and A. Starinets, Phys. Lett. B **454** (1999), 77 , hep-th/990385.
- 16) D. Z. Freedman, S. S. Gubser, K. Pilch and N. P. Warner, Adv. Theor. Math. Phys. **3** (1999) 363, hep-th/9904017.
- 17) Y. Nambu, “Duality and Hydrodynamics”, Lecture Notes at the Copenhagen Symposium (unpublished), 1970.
- 18) T. Goto, Prog. Theor. Phys. **46** (1971), 1560.
- 19) A.M. Polyakov, Phys. Lett. B **103** (1981), 207.
- 20) S. Ichinose, Phys. Lett. B **152** (1985), 56.
- 21) J. Schwinger, Phys. Rev. **82** (1951) 664.
- 22) P. A. M. Dirac, *The Principles of Quantum Mechanics*, 4th Edition (Oxford Univ. Press, Oxford, 1958).
- 23) E. A. Mirabelli and M. E. Peskin, Phys. Rev. D **58** (1998), 065002 , hep-th/9712214.
- 24) S. Ichinose and A. Murayama, Nucl. Phys. B **710** (2005), 255 , hep-th/0401011.
- 25) S. Ichinose, “Casimir and Vacuum Energy of 5D Warped System and Sphere Lattice Regularization”, Proc. of VIII Asia-Pacific Int. Conf. on Gravitation and Astrophysics ,ed. M. Kenmoku and M. Sasaki (ICGA8, Aug. 29-Sep. 1,2007, Nara Women’s Univ., Japan), p36, arXiv:/0712.4043.
- 26) S. Ichinose, Int. J. Mod. Phys. **23A** (2008), 2245 ; Proc. of the Int. Conf. on Prog. of String Theory and Quantum Field Theory ,ed. K. Fujiwara et al (Dec. 7-10, 2007, Osaka City Univ., Japan), arXiv:/0804.0945.
- 27) S. Ichinose, “Casimir Energy of AdS5 Electromagnetism and Cosmological Constant Problem”, Talk at Int. Conf. on “Particle Physics, Astrophysics and Quantum Field Theory: 75 Years since Solvay” (PAQFT08,Nov. 27-Nov. 29, 2008, Nanyang Executive Center, Singapore), to appear in the conference proceedings, arXiv:/0903.4971.
- 28) S. Ichinose, “Casimir Energy of 5D Warped System and Sphere Lattice Regularization”, arXiv:/0812.1263(hep-th).
- 29) R. P. Feynman, *Statistical Mechanics*, (W. A. Benjamin, Inc., Massachusetts, 1972).
- 30) T. Yoneya, “Duality and Indeterminacy Principle in String Theory” in *Wandering in the Fields*, ed. K. Kawarabayashi and A. Ukawa (World Scientific, 1987), p. 419.  
T. Yoneya, “String Theory and Quantum Gravity” in *Quantum String Theory*, ed. N. Kawamoto and T. Kugo (Springer, 1988), p. 23.  
T. Yoneya, Prog. Theor. Phys. **103** (2000), 1081.
- 31) S. Wolfram, *The Mathematica Book*, 4th ed., (Wolfram Media/Cambridge University Press, 1999).